Discovery of Novel Adenosine Receptor Antagonists through a Combined Structure- and Ligand-Based Approach Followed by Molecular Dynamics Investigation of Ligand Binding Mode

Panagiotis Lagarias,[†] Eleni Vrontaki,[†] George Lambrinidis,[†] Dimitrios Stamatis,[†] Marino Convertino,[‡] Gabriella Ortore,[§] Thomas Mavromoustakos,[≠] Karl-Norbert Klotz,[⊥] Antonios Kolocouris[†,*]

[†] Division of Pharmaceutical Chemistry, Department of Pharmacy, School of Health Sciences, National and Kapodistrian University of Athens, Panepistimiopolis-Zografou, 15771 Athens, Greece

[‡] Department of Biochemistry & Biophysics, University of North Carolina at Chapel Hill, 120 Mason Farm Road, Chapel Hill, NC 27599, USA

[§] Department of Pharmacy, University of Pisa, 56126 Pisa, Italy

[≠] Division of Organic Chemistry, Department of Chemistry, School of Science, National and Kapodistrian University of Athens, Panepistimiopolis-Zografou, 15771 Athens, Greece

[⊥] Institute of Pharmacology and Toxicology, University of Würzburg Versbacher Str. 9 97078 Würzburg, Germany

1/25/2019

1 Abstract

An intense effort is made by pharmaceutical and academic research laboratories to identify and develop selective antagonists for each adenosine receptor (AR) subtype as potential clinical candidates for "soft" treatment of various diseases. Crystal structures of subtypes A_{2A} and A_1ARs offer exciting opportunities for structure-based drug design. In the first part of the present work, Maybridge HitFinder^{TM} library of 14400 compounds was utilized to apply a combination of structure-based against the crystal structure of A_{2A}AR and ligand-based methodologies. The docking poses were re-scored by CHARMM energy minimization and calculation of the desolvation energy using Poisson-Boltzmann equation electrostatics. Out of the eight selected and tested compounds, five were found positive hits (63% success). Although the project was initially focused on targeting the A_{2A}AR, the identified antagonists exhibited low micromolar or micromolar affinity against A_{2A}/A_3 ARs or A_3AR, respectively. Based on these results, 19 compounds characterized by novel chemotypes were purchased and tested. Sixteen of them were identified as AR antagonists with affinity towards combinations of the AR family isoforms (A_{2A}/A_3, A_1/A_3, $A_1/A_{2A}/A_3$ and A_3). The second part of this work involves the performance of hundreds of molecular dynamics (MD) simulations of complexes between the ARs and the total of 27 ligands to resolve the binding interactions of the active compounds, which were not achieved by docking calculations alone. This computational work allowed the prediction of stable and unstable complexes which agree with the experimental results of potent and inactive compounds respectively. Of particular interest is that the 2-amino-thiophene-3-carboxamides, 3-acylamino-5-aryl-thiophene-2-carboxamides and carbonyloxycarboximidamide derivatives were found to be selective and possess a micromolar to low micromolar affinity for A_3 receptor.

2 Introduction

Adenosine receptors (ARs) belong to the family of G protein-coupled receptors (GPCRs) and are expressed in both the CNS and the periphery. The four AR subtypes (A_1, A_{2A}, A_{2B} and A_3) are responsible for a wide range of physiological processes by acting upon different signaling pathways. The A_{2A} and A_{2B} ARs increase 3′,5′-cyclic adenosine monophosphate (cAMP) levels by coupling to G_s, whereas the A_1 and A_3AR subtypes signal via G_i and decrease cAMP. [1,2] Adenosine is involved in the regulation of several biological functions in different organs and tissues, including the CNS, the cardiovascular system and the airways; many pathophysiological states are associated with changes of adenosine levels. [3] For these reasons, selective agonists, antagonists and allosteric enhancers [4] provide promising clinical candidates. Indeed, therapeutic modulation of the adenosine system could offer the possibility of a "soft" treatment of different diseases, but due to the ubiquitous distribution of adenosine and its receptors, the challenge in ligand development depends on the specificity for the different receptor subtypes. A_2AR antagonists have emerged as an attractive approach to treat Parkinson, sickle cell and infectious diseases, cancer, ischemia reperfusion injury, diabetic nephropathy, cognition and other CNS disorders. [5,6,7,8,9] A_{2B}AR antagonists may be useful for the treatment of asthma, chronic obstructive pulmonary disease (COPD) and inflammation. [10,11,12] The A_1AR is also an attractive pharmacological target. Its antagonists have been explored as kidney-protective agents, cognitive enhancers, anti-asthmatic and CNS agents. [13] Finally, A_3AR-selective antagonists are of interest for therapeutic applications in asthma, glaucoma, COPD etc. [14]

A breakthrough in the AR field was the publication of a crystal structure for the A_{2A} subtype, which revealed the binding mode of the antagonist 4-[2-[7-amino-2-(2-furyl)-1,2,4-triazolo-[1,5-a][1,3,5]triazin-5-ylamino]ethyl]phenol (ZM241385) (Figures S1, S2). [15,16] This enabled the use of remarkably successful structure-based approaches in ligand discovery providing high hit rates and novel ligands using A_{2A}AR [17,18,19,20,21,22,23,24,25,26] and homology models of A_1 and A_3AR derived therefrom. [27,28] In these studies, the ligand recognition occurs in the upper region of the transmembrane (TM) bundle, and the bound ligand is surrounded by TM3, 5, 6, and 7 and occasionally by TM2. The bound ligands are anchored inside the same binding cleft for all AR subtypes and can form up to two stabilizing hydrogen bonds with the side chain amide group of the N(6.55) [29,30] in TM6 (numbers in parentheses refer to the Ballesteros–Weinstein numbering[31]). The importance of interactions with N(6.55) was identified early in docking screenings. [18] N(6.55) and L(6.51) are key-to-recognition and highly conserved residues in all four AR subtypes and have been found to be crucial interaction

partners for both agonists and antagonists in mutagenesis studies. [29] The ligands can occasionally form a tight hydrogen bond with the carboxylate group of E(5.30) in the extracellular loop 2 (EL2) in A_1, A_{2A} and A_{2B}ARs (see Figure S1). The recently published crystal structures of the A_1AR bound to the selective covalent antagonist 8-cyclohexyl-3-(3-(4-fluorosulfonylbenzamido)propyl)-1-propylxanthine (DU172) [32] or 1-butyl-3-(3-hydroxypropyl)-8-(3-noradamantyl)xanthine (PSB36) [33] (Figure S2) can be utilized also for structure-based drug design and new insights into the selectivity of ligands against ARs.

Although the docking campaigns applying convenient scoring functions were successful, [34] molecular mechanics Poisson-Boltzmann surface area (MM-PBSA) methods which account for ligand and the protein solvation before and after binding using an implicit solvation model [35] improved scoring significantly. [36,37,38,39] Since the AR-ligand complexes have considerable therapeutic impact, strategic longer MD simulation studies have been performed in order to test the effect of the starting conformation of the ligand, [40] the effect of protein flexibility on the binding conformation of the ligand, [41] the contribution of the lipid bilayer to the protein conformational space, [42] the conformational transition at long simulation times, [43,44] recognition pathways of the ligand [45] etc. The molecular binding interactions derived from structure-based virtual screening against ARs are often described better through all-atom MD simulations of the protein complexes. [19]

Here, we explored the *in silico* screening of 14400 compounds included by Maybridge HitFinder library [46] against the X-ray structure of A_{2A}R complexed with ZM241385 using a combination of structure-based and ligand-based approaches. The re-scoring of a subset of docking poses was performed with CHARMM-PBSA energy minimization to further account for desolvation energy. Eight compounds were selected and tested and five of them were identified as positive hits. Compounds **1** and **5** exerted low micromolar affinities against A_{2A}/A_{3A}Rs (Table 1). Compound **2** exhibited micromolar affinity against A_3AR and a very weak affinity against A_{2A}AR and compounds **6** and **7** micromolar affinity against A_3AR. Based on the structure of the three most promising compounds, 19 new compounds were purchased, of which 16 were found to be binders to ARs. Compounds **12**, **14** and **23** exhibited affinity for A_{2A}/A_3, compounds **15**, **21** and **26** for A_1/A_3, compounds **13**, **16** and **17** for $A_1/A_{2A}/A_3$, compound **27** for A_1, and the eight compounds **9-11**, **18**, **20**, **22**, **24**, **25** were selective for A_3. Molecular docking calculations and MD simulations of the 27 ligands against A_1, A_{2A}, A_{2B} and A_3ARs were employed in an attempt to provide clues about the compounds' binding interactions. Interestingly, the 27 tested ligands resulted in similar docking poses against A_1, A_{2A}, A_{2B} or A_3ARs. Thus, MD simulations of numerous complexes (which are possible only using supercomputers), have been applied to investigate further the basic binding interactions of the active

compounds. In particular, over two hundreds short (10 ns) MD simulations were performed with Desmond [47,48] using OPLS 2005 [49,50,51] force field to relax ligand-receptor interactions. When the MD simulations resulted in a binding orientation similar to the docking pose (RMSD$_{lig}$ < 1.5 Å) the stability of the AR-ligands complexes was verified by performing longer (100 ns) MD simulations with Desmond [47,48] using OPLS 2005 [49,50,51] force field and with Amber [52] using ff14SB [53] to model all protein and ligand interactions. A work flow of the computational methods used is presented in Scheme 1. The eight A$_3$AR-selective compounds provide novel chemotypes which may find use in various human pathologies.

3 Materials and Methods

Molecular docking and scoring calculations of the Maybridge HitFinder library

Ligand Preparation

Prior to the docking calculations, the Maybridge HitFinder library [46] was prepared using the LigPrep workflow as implemented on Maestro 10.3 (Schrödinger Release 2016-3: LigPrep, Schrödinger, LLC, New York, NY, 2016). The initial 14400 structures gave 19229 tautomers. Those tautomers were subjected to conformational analysis using OMEGA software (OpenEye Inc) [54,55] resulting in 1655368 conformers which were used for virtual screening.

Virtual Screening

The molecular docking calculations were carried out using the 2.6 Å resolution crystal structure of the human A$_{2A}$AR in complex with the antagonist ZM241385 (PDB ID 3EML). [15] This virtual screening project started just before any other X-ray structure was published. [16,21,56,57] Among the crystal structures of A$_{2A}$AR-antagonist complexes released after 3EML, PBD ID 4EIY [57] contained also co-crystallized ZM241385 possessed the highest 1.8 Å resolution. Both the desolvation energy for inserting a compound into the receptor and its attractive interactions with the orthosteric binding area of A$_{2A}$AR were used as contributions to energy during hit selection. In this context, the shape and coordinates of the critical amino acid side chains participating to interactions with the ligands inside the binding site, do not differ essentially between 3EML and the other newer released structures, for

example 3PWH (3.3 Å), or the highest in resolution 4EIY. Figure S3 shows the superposition of 3EML, 4EIY and 3PWH. The highest resolution receptor structure 4EIY is nearly identical to the original 2.6 Å resolution crystal structure 3EML with an all-atom RMSD of 0.45 Å to 81% of $A_{2A}AR$. Recently, it was reported that a virtual screening performed against $A_{2A}AR$ using two different X-ray structures (PDB ID 4EIY, 3PWH) resulted in 11 ligands with affinity to $A_{2A}AR$. [26] Five were identified from docking using Glide and structure 4EIY and six were identified by the Glide docking based on structure 3PWH, i.e., the virtual screening based on the two crystal structures produced different hits. Nevertheless, we did not test a second virtual screening using 4EIY or other protein co-crystallized structure of AR with a ligand.

Using 3EML structure, the complex was prepared for the calculations by removing all non-protein atoms and the intracellular T4-lysozyme insertion. The most favoured protonation states of ionizable residues (D, E, R, K and H) at pH 7 were assigned using Maestro. [58] The protonation states of the histidines in the binding region were set according to literature data in order to contribute to the stabilization of complexes. His7.43 was protonated at epsilon position to form H-bonds with the ligands (see for example Figures 4c, 6b). His6.52 was protonated at the epsilon position so as to form possible interactions with waters according to the literature. His6.66, at the top of the ligand binding site, was doubly protonated to form a salt-bridge with Glu5.30 in A_{2A} and A_1AR subtypes; in A_3AR it was protonated at the delta position to avoid repulsive interactions since A_3AR has a Val instead of Glu5.30. The N- and C-termini of the protein were capped by acetyl and methylamino groups, respectively, after applying the protein preparation module of Maestro. [40,58] All hydrogens atoms of the protein-ZM241385 complex were minimized with the AMBER* force field by means of Maestro/Macromodel 9.6 using a distance-dependent dielectric constant of 4.0. The MM minimizations were performed with a conjugate gradient (CG) method and a root mean square of the energy gradient (threshold) value of 0.0001 kJ $Å^{-1}$ mol^{-1} was used as the convergence criterion. The *apo*-protein and ZM241385 structures were saved separately and used for the subsequent docking calculations. Molecular docking was performed with GOLD 5.2. [59,60,61] The ligand binding site was defined within 15 Å of the native ligand in the receptor structure. Comparison of the best docking poses obtained with GoldScore, [60] ChemScore [62] and ChemPLP [63] afforded an RMSD of of 1.1 Å, 4 Å and 0.80 Å respectively for ZM241385, relative to the X-ray coordinates [15]. Therefore, further docking calculations were performed using the ChemPLP [63] scoring function. The energy minimized ligands structures were submitted to ten genetic algorithm runs which is the default value used by the GOLD program. The "allow early termination" command was activated (which terminates searching for a ligand if the top three solutions have an RMSD difference in their coordinates smaller than 1.5 Å) and

the docking poses were clustered using an RMSD difference criterion of 1.5 Å. All other parameters were set to their default values. In total, 48230 clusters and representative docking poses (Scheme 1) were selected.

3D Similarity Calculations

The ligand-based virtual screening tool Rapid Overlay of Chemical Structures (ROCS) [64] was used to predict structures that were similar to ZM241385 (molecular query). In brief, the docking poses of each compound were superimposed and scored on the basis of their overlap with the query in terms of shape (ShapeTanimoto) and functional groups (ColorTanimoto). All of the 3D similarity calculations were ranked according to the TanimotoCombo metric, which is the sum of the ShapeTanimoto and ColorTanimoto scores and thus ranges from 0 to 2. The top 6000 solutions (TanimotoCombo coefficient > 0.65) were selected for re-scoring using the MM-PBSA method as follows.

CHARMM-PBSA re-scoring

Energy minimization. Complexes of 6000 docking poses with A_2AR were subjected to MM-PBSA calculations using the CHARMM program [65,66] after applying a software for fragment-based molecular docking and protein structure preparation created by the A. Caflisch group. [67] All ligand-protein complexes were minimized with the CHARMM27 force field by the CG algorithm to a threshold value of 0.001 kcal mol^{-1} Å^{-1}. During minimization, the electrostatic energy term was screened by a distance-dependent dielectric of 4r to prevent artificial deviations due to vacuum effects and the default nonbonding cutoff of 14 Å was used. Protein atoms were kept fixed. The minimized structures were used for evaluating the van der Waals and Coulomb energy, and solvation energies using finite-difference Poisson calculations.

Binding Energy Calculations. The van der Waals and electrostatic interaction energies were calculated by subtracting the values of the isolated components from the energy of the complex. The van der Waals energy was calculated with CHARMM27 force field using the default cutoff of 14 Å. The electrostatic energy is the sum of the Coulomb energy in vacuum and the solvation energy. The electrostatic energy was calculated with CHARMM [66] using infinite cutoff and neglecting interactions between pairs of atoms separated by one or two covalent bonds. The electrostatic solvation energy was calculated by the finite-difference Poisson approach [68] using the PBEQ (Poisson-Boltzmann equation) module [69] in CHARMM and a focusing procedure with a final grid spacing of 0.3 Å. The size of the initial grid was determined by considering a layer of at least 20 Å around the solute. The dielectric

discontinuity was delimited by the molecular surface spanned by a rolling probe of 1.4 Å. The ionic strength was set to zero, and the temperature to 300 K. Two finite-difference Poisson calculations were performed for each of the three systems (ligand, protein, and ligand-protein complex). The solvation energy is the difference between the values from calculations between ligand-protein complex and ligand and protein alone. The exterior dielectric constant was set to 78.5 and 1.0 in the first and second calculation, respectively, while the solute dielectric constant was set to 1.0, which is consistent with the value used for the parameterization of the charges and the membrane-protein environment. Eight compounds were selected for testing based on their synthetic feasibility and structural availability (see Table S1) of which five were identified to be positive hits.

Calculations of the tested ligand - AR complexes

Models for A_1, A_{2A}, A_3 and A_{2B}ARs. For calculations of the complexes between ligands and A_{2A}AR or A_1AR, the X-ray structure of hA_{2A}AR (PDB ID 3EML [15]) and the recent X-ray structure hA_1AR (PDB ID 5UEN [32]) were respectively used. Since there are no crystal structures available for A_{2B} and A_3ARs , their homology models developed by Katritch and Abagyan [70] were used for the relevant calculations. Additionally, the homology models of of A_{2B} and A_3ARs available from the Adenosiland server of Moro were used. [71] Structures in Adenosiland of Moro [71] included all residues and did not need any additions. The homology models were built using the crystal structure of the hA_{2A}AR (PDB ID 3EML [15]) as a template. These receptor structures were used directly for the docking calculations, without the addition of any missing residues. In order to obtain suitable structures of AR-ligand complexes for performing MD simulations, missing portions of the A_1, A_{2A}, A_{2B} and A_3AR structures were generated with the software MODELLER. [72,73] The missing residues in the crystal structure of A_{2A}AR (PDB ID 3EML [15]) i.e., M1-I3 (N-terminus), P149−H155 (extracellular loop 2, EL2), and K209-A221 (intracellular loop 3, IL3) were added. The final structure lacks the C-terminus and contains only residues 1 to 310. A similar procedure was followed for A_1AR. It should be noted that the Katritch-Abagyan [70] structures were optimized by taking into account the binding energies from molecular docking calculations and the experimental selectivity of ligands for the four AR subtypes.[70,71] In Katritch-Abagyan [70] structures of the A_3 and A_{2B}ARs the portion that corresponds to the EL2 between positions L4.62 and C5.27 is missing. [72,73] As it has been reported, EL2 may orchestrate a network of interactions that can stabilize the inactive conformation of the receptor and/or kinetically control the receptor-ligand recognition. [74,75] A_{2B} subtype is characterized by the longest

EL2, while A_3 subtype by the shortest. [76] Despite the high degree of structural diversity with respect to EL2 in family A GPCRs, there is one feature that is conserved in the vast majority of them, that is the disulfide bond between EL2 and C3.25 at the top of TM3. This disulfide bond effectively tethers EL2 on the top of the TM helical bundle and imposes a very important conformational constraint upon EL2. Some GPCRs have additional disulfide bonds between different ELs such as between EL2-EL1 found in all A_{2A} subtype receptors. [77] Furthermore, the A_{2A}AR subtype possesses an additional intra-loop disulfide bond, within EL3, in common with melanocortin receptors and human histamine receptor 1. These "additional" disulfide bonds contribute in reducing the flexibility of ELs and, as a consequence, they peculiarly sculpt the topography of the extracellular portion of the receptor proximately to the orthosteric binding cleft.

It has been shown that the A_1AR binding area is broader compared to that of A_{2A}R, including a secondary binding region next to the common orthosteric one. The compact structure of the TM bundle in A_{2A}AR is consistent with its unique disulphide bond (C74-C146) through which the beginning of TM3 is tightly connected to the end of EL2 allowing shifts in TM1, 2, and 3 as suggested in ref. 32 and in this work. Both A_1 and A_3AR lack this disulphide bond. According to ref. 32, TM7 tilts towards TM6, possibly as a result of a shorter EL3 in A_1AR owing to the deletion of one amino acid; EL3 is also one amino acid shorter in A_3AR compared to A_{2A}AR. These differences in tethering of the ELs result in the different shapes of the binding sites.

Almost all AR subtypes contain an E(5.30) residue, except A_3AR which contains a V(5.30). This glutamic acid residue may play an important role in high affinity ligand binding through the formation of a hydrogen bond, for example, with an unsubstituted exocyclic amine. Having a valine substituting this position, A_3AR lacks this interaction and therefore allows bulky amine substitutions or neighbouring lipophilic fragments to protrude towards the extracellular opening of the pocket. Katritch and Abagyan reported [70] that some valine rotamers can also partially block this opening, thus using an optimized conformational model of the receptor may be required for specific investigation of ligand binding against A_3AR.

Docking calculations. The structures of ligands **1-27** (Table 1) were built by means of Maestro 8.5 and were subsequently minimized by means of Macromodel 9.6 and the MMFF94 force field [78,79] using the CG method and a distance-dependent dielectric constant of 4.0 until a convergence value of 0.0001 kJ Å^{-1} mol^{-1} was reached. The 27 ligands depicted in Table 1 were subjected to docking calculations with Gold5.2 [59,60,61] using both the GoldScore [60] and ChemPLP [63] scoring functions. Regarding the complexes with A_{2A}AR and A_1AR the PDB IDs 3EML [15] and 5UEN [32] were respectively used. The homology models of both Moro and Katritch-Abagyan were used for the A_3 and

A$_{2B}$ARs. The binding site for the docking calculations of the 27 ligands was defined using the coordinates of ZM241385 in A$_{2A}$AR (PDB ID 3EML [15]) which was selected as reference ligand. All protein atoms within 10.0 Å of the selected ligand were used in the binding site definition. The ligands were submitted to 10 genetic algorithm runs. Docking poses for each ligand were visualized using the UCSF Chimera package. [80] The tested molecules **1-27** resulted in similar docking poses against A$_1$, A$_{2A}$, A$_{2B}$ or A$_3$ARs independently of the protein model used and scoring function. Thus, MD simulations were performed to investigate the basic binding mode features for compounds exhibiting affinity to the above mentioned receptors.

MD simulations. MD simulations for 10 ns were performed for ligands **1-27** (Table 1) complexed at A$_{2A}$, A$_1$, A$_3$ and A$_{2B}$ARs, and embedded in hydrated POPE bilayers. [42] The docking poses of ligands 1-27 inside the othrosteric binding site of A$_{2A}$, A$_1$, A$_3$ and A$_{2B}$ARs were used as starting structures. The ligands are allowed to relax close atom contacts and adopted a more favorable binding orientation. [43] The choice between DMPC, POPE and POPC as the model membrane bilayer for the MD simulations, was based on test calculations. 70 ns MD simulations for ZM241385-A$_{2A}$ complex in the different lipid bilayers were applied. POPE bilayers resulted in the smallest displacement (RMSD) from the crystallographic coordinates (see Figures S4, S5). For the comparison to be reliable, the average area per lipid head group in each lipid model was measured for each bilayer system at the end of the MD trajectory and was compared to the experimental values. The area per lipid was measured based on a combination of the two-dimensional Voronoi tessellation and the Monte Carlo integration method. [81] The time courses (Figure S6) and measures (Table S2) obtained, provided consistent values with the experimental ones for pure lipid bilayers suggesting that the membranes were properly equilibrated. More than two hundred MD simulations, performed in duplicate for each complex, were performed in supercomputers using Desmond [47,48] with OPLS 2005 force field. The duration of each MD simulation was 10 ns and the RMSD of the ligand inside the binding site was measured with respect to its docking pose coordinates (see RMSD$_{lig.}$ values in Table S3). We observed complexes where the ligand escapes from the orthosteric binding area and the RMSD$_{lig.}$ value was in most of the cases ≥ 4 Å at the end of the simulation, and complexes in which the ligand retained a binding orientation similar to the starting docking pose where the RMSD$_{lig.}$ value was 2-3 Å. In the latter cases, the stability of the complex was further verified by extending the simulation time to 100 ns (see Table S3). [49,50,51] The stability of the ligand-AR complexes was verified for ligands **1, 2, 5, 12, 13, 14, 16, 17, 23** to A$_{2A}$AR, ligands **13, 15, 16, 17, 21, 26, 27** to A$_1$AR and ligands **1, 2, 5, 6, 7, 9-18, 20-25, 27** to A$_3$AR. Figures 1-7 depict the binding orientations of representative complexes. To further test the stability of these complexes, 100 ns MD simulations were performed on the representative

complexes **1**-A$_{2A}$, **1**-A$_3$, **5**-A$_{2A}$, **5**-A$_3$, **13**-A$_{2A}$, **11**-A$_3$, **17**-A$_{2A}$, **17**-A$_1$ and **17**-A$_3$ using Amber with ff14SB force field for the ligand-protein complex [53] and lipid14 parameters for the lipid (Scheme 1). [82]

The procedure applied for the MD simulations was the following. The N- and C-termini of the protein model systems were capped by acetyl and methylamino groups, respectively, after applying the protein preparation module of Maestro. The AR complex was embedded in a POPE lipid bilayer extending 15 Å beyond the solute. The ligand-receptor complex was placed into the membrane according to the orientation with respect to the membrane plane (x-y plane) suggested by the "Orientations of Proteins in Membranes (OPM)" server. [83] Complex and lipid systems were solvated using the TIP3P [84] water model. Na$^+$ and Cl$^-$ ions were placed in the aqueous phase to neutralize the systems and reach the experimental salt concentration of 0.150 M NaCl. The total number of atoms in each system was approximately 81770. Membrane generation and system solvation were conducted with the "System Builder" utility of Desmond. [47,48] The OPLS 2005 force field [49,50,51] was used to model all protein-ligand interactions and lipids. The particle mesh Ewald method (PME) [85,86] was employed to calculate the long-range electrostatic interactions with a grid spacing of 0.8 Å. Van der Waals and short-range electrostatic interactions were smoothly truncated at 9.0 Å. The Nosé-Hoover thermostat [87] was utilized to maintain a constant temperature in all simulations, and the Martyna-Tobias-Klein method [87] was used to control the pressure. Periodic boundary conditions were applied and the dimensions of the simulation box were (80×95×110) Å^3. The equations of motion were integrated using the multistep RESPA integrator [88] with an inner time step of 2 fs for bonded interactions and non-bonded interactions within a cutoff of 9 Å. An outer time step of 6.0 fs was used for non-bonded interactions beyond the cut-off. Each system was equilibrated using a modification of the default protocol provided in Desmond. The modification of the protocol consists of a series of restrained minimizations and MD simulations designed to relax the system, while not deviating substantially from the initial coordinates. First, two rounds of steepest descent minimization were performed using a maximum of 2000 steps and harmonic restraints of 50 kcal mol Å^{-2} applied on all solute atoms, followed by 10000 steps of minimization without restraints. The first simulation was run for 200 ps at a temperature of 10 K in the NVT (constant number of particles, volume, and temperature) ensemble with solute heavy atoms restrained by a force constant of 50 kcal mol Å^{-2}. The temperature was then raised during a 200 ps MD simulation to 310 K in the NVT ensemble with the force constant retained. The temperature of 310 K was used in MD simulations in order to ensure that the membrane state is above the main phase transition temperature of 298 K observed for POPE bilayers. [89] The heating was then followed by equilibration simulations. First, two 1 ns stages of NPT equilibration (constant number of particles, pressure, and temperature) were performed. In the first 1

ns stage, the heavy atoms of the system were restrained by applying a force constant of 10 kcal mol $Å^{-2}$ for the harmonic constraints and in the second 1 ns stage the heavy atoms of the protein-ligand complex were restrained by applying a force constant of 2 kcal mol $Å^{-2}$ to equilibrate solvent and lipids. This equilibration protocol was followed by 10 ns simulation without restraints in POPE. For stable complexes, the NPT simulation time was extended to a 100 ns.

Regarding the calculations using Amber software, after the protein ligand-complex was inserted to the POPE bilayer according to the procedure reported above, [83] the systems were processed by the LEaP module in AmberTools14, [52] where Amber ff14SB force field parameters [53] were applied to the protein and lipid14 [82] to the lipids and TIP3P [84] to the water molecules. As for the ligands, the atomic charges were calculated using the R.E.D. Server development [90] along with PARM10 parameters. [91] NPT simulations were performed on the protein-membrane systems using the GPU implementation of the AMBER 12 code, [52] after a short energy minimization and equilibration in the NVT ensemble. The equilibration was followed by a 100 ns NPT simulation without restraints.

All the MD simulations were run on ARIS and CyTERA Supercomputing Systems or in workstations using the GPU implementation of the MD simulations codes.

The X-ray structures of A_{2A}-ZM241385 and A_1AR-DU172 complexes and the relevant Katritch-Abagyan [70] or Moro A_{2A} and A_1AR structures when subjected to MD simulations for 10 ns in POPE bilayers resulted to similar structures as demonstrated by RMSDs $\leq$ 2 Å for Cα-carbons. Similar structures were acquired after the MD simulations for representative A_3AR-ligand complexes using either the A_1 or $A_{2A}AR$ experimental structure for building the homology model. The A_3AR binding area was found to be broader than that of $A_{2A}AR$ as mentioned in ref. 70 due to the absence of the disulphide bond C74-C146 and tethering of TM3 with EL2.

2D Similarity Calculations

Similarity calculations for ligands were carried out using the Canvas program by Schrödinger. [92] In order to investigate the novelty of the discovered hits, we calculated the maximum pairwise Tanimoto similarity of each hit in respect to the thousands of known AR ligands in the ChEMBL22 database using the extended chemical fingerprints for four atoms (ECFP4). [93,94] (see Table S4). The Tanimoto coefficient (Tc) quantifies the two-dimensional chemical similarity between two molecules by adopting a value between 0 and 1.

Pharmacological Characterization

Radioligand Binding Studies at human A_1, A_{2A} and A_3ARs

All pharmacological methods followed the procedures as described in the litarature. [95] In brief, membranes for radioligand binding were prepared from CHO cells stably transfected with hAR subtypes in a two-step procedure. In the first step, cell fragments and nuclei were removed at 1000 x g and then the crude membrane fraction was sedimented from the supernatant at 100000 x g. The membrane pellet was resuspended in the buffer used for the respective binding experiments and it was frozen in liquid nitrogen and stored at -80 °C. For radioligand binding at the hA_1AR, 1 nM [^{3}H]CCPA was used, for $hA_{2A}AR$ 10 nM [^{3}H]NECA and for hA_3AR 1 nM [^{3}H]HEMADO. Non specific binding of [^{3}H]CCPA was determined in the presence of 1 mM theophylline and in the case of [^{3}H]NECA and [^{3}H]HEMADO 100 μM R-PIA was used. [96] K_i values from competition experiments were calculated using the program Prism (GraphPad Software, La Jolla, CA, U.S.A.) assuming competitive interaction with a single binding site. The curve fitting results (see Figure 8) showed R^2 values $\geq$ 0.99 for all compounds and receptors, indicating that the used one-site competition model assuming a Hill slope of n=1 was appropriate. The affinity of the ligands is depicted in Table 1.

Adenylyl cyclase activity

The potency of antagonists at the $hA_{2B}AR$ was determined by adenylyl cyclase experiments. The procedure was carried out as described previously with minor modifications. [95,97] Membranes were prepared from CHO cells stably transfected with $hA_{2B}AR$ using only one high speed centrifugation of the homogenate. The resulting crude membrane pellet was resuspended in 50 mM Tris/HCl, pH 7.4 and immediately used for the cyclase assay. Membranes were incubated with about 150000 cpm of [a-32P]ATP for 20 min in the incubation mixture as described without using EDTA and NaCl. [97] None of the compounds showed measurable interaction with $A_{2B}AR$, as the IC_{50}-values for concentration-dependent inhibition of NECA-stimulated adenylyl cyclase were all > 30 μM.

4 Results and Discussion

Molecular docking, scoring and selection of compounds for testing

Molecular docking calculations were applied to 14400 compounds (included in the HitFinder collection of Maybridge) against an $A_{2A}AR$ crystal structure (PDB ID 3EML) [15] after generating 200 conformations for each ligand using the program OMEGA (see Scheme 1 and Materials and Methods Section). [55] The docking calculations were performed on the resulting library (1655368 conformers) with GOLD5.2 [59,60,61] and ChemPLP [63] was used as the scoring function to produce 48230 clusters of docking poses. These were overlaid onto the crystallographic ZM241385 conformation adopted inside the crystal structure of $A_{2A}AR$ [15] using ROCS [98] which relies on the detection of molecules with 3D properties similar to those of the reference compound. The top 6000 conformers were re-scored by a CHARMM-PBSA minimization (see Table S1). This last filtering was very important since the docking poses from the previous step had similar polar and vdW contacts. The top 60 docking poses from 60 different compounds were selected and eight compounds were purchased based on the structural versatility and synthetic feasibility. From the eight compounds tested (Scheme 1) five were found to be positive hits (62.5% success) showing mixed antagonistic activity against ARs with affinities $\leq$ 20-30 μM. Remarkably, none of these eight positive hits was among the 60 after just applying: a) docking with GOLD and scoring with ChemPLP, and b) filtering with ROCS using scoring based on T_c (see Table S5). Thus, the CHARMM-PBSA re-scoring step which accounts for the desolvation energy needed in order the ligand to reach the receptor binding area was significant for ligands filtering. Several approaches were also applied in previous virtual screening attempts for improving ligand enrichment. These works include a combination of scoring tools for filtering. In the first campaigns, an optimized docking protocol was applied [18] or a docking and scoring using DOCK program which also accounted for the desolvation penalty.[17] Other groups applied also a docking/scoring using DOCK which accounted for the desolvation penalty [19] [27] or applied GlideSP/XP and other tools like induced fit docking.[22] In a recent effort after docking and scoring with Glide/SP, REOS/Knime filtering was applied and then MM-GBSA calculations were performed which account for the desolvation penalty; in this particular effort after testing 79 compounds only two were found to meet the criterion of approximately 50 % radioligand displacement at a concentration of 10 μM. [25]

ARs are not easy targets for achieving selectivity since they have broad and similar orthosteric binding sites. Thus, it is not a surprise the fact that a research targeting a particular AR subtype can

lead to antagonists of another AR subtype. A characteristic example that illustrate this point, is the virtual screening campaign starting with four separate homology models of the human A_1AR and docking of 2.2 million compounds to all four models. Thirty-nine (39) hits were selected and tested for their binding in three AR subtypes. They were found to bind to two or three AR subtypes resulting in 21% A_1, 38% A_{2A} and 36% A_3AR successful antagonist hits. [27]

Nineteen (19) molecules were selected from the e-molecules search engine, based on their similarity to the structures of compounds **1**, **2** and **5**, which are the most accessible with regards to their chemical synthesis. In particular, compounds **9-13** were selected based on the structure of **1**. Compounds **1**, **9-13** contain an amino group at 2-thiophene position and an amido (CONHR) group at 3-thiophene position. Compared to **1**, and **9-13** compounds **14-18, 26, 27** were selected to contain the $CONH_2$ group at 2-thiophene position and the NHCOR' group at 3-thiophene position. Compound **19** was selected to resemble structure **2** and **20-25** were selected based on the structure of **5**. The results from testing of compounds **9-27** are depicted in Table 1 and show that 23 compounds out of the 27 compounds are binders of various combinations of ARs with weak to potent antagonistic activity. Thus their K_i values ranged from 61 μM to submicromolar values. Overall, out of all 27 compounds included in Table 1 only four compounds lack affinity against any ARs (**3**, **4**, **8**, **19**). The model used to fit the binding data and determine K_i values confirms competitive interaction with the receptors (see Figure 8). [99]

Compounds classification, binding assays results and novelty

Compounds classification and affinity results

The 27 compounds can be categorized according to their structural similarity characteristics in five classes (A-E), or in four classes according to receptor selectivity, i.e. ligands with affinity only against A_3, against A_{2A}/A_3, against A_1/A_3, and against $A_1/A_{2A}/A_3$ ARs.

Class A: Class A includes 2-amino-thiophene-3-carboxamides **9-11** and 2-amino-5-phenyl-3-thiophenecarbohydrazides **1**, **12** and **13.** Derivatives **9**, **10** and **11** exhibited binding only to A_3AR, with corresponding K_i values being 16.5, 14.8 μM, while **9** possess a weak affinity with $K_i = 37.1$ μM. The addition of a condensed cyclopentane or cyclohexane ring to the thiophene ring in **9**, resulted in **10** and **11** respectively, which exhibited ~ two-fold increased affinity (Table 1). When a 3-phenyl group was added to the thiophene ring, the resulting 2-amino-5-phenyl-3-thiophenecarbohydrazide derivatives **12** and **1** exhibited affinity for A_{2A}/A_3AR with K_i values 3.93, 5.77 μM and 2.67, 3.10 μM respectively, or

in the case of **13** against $A_1/A_{2A}/A_3AR$ (K_i values 15.2, 4.59, 5.16 μM).

Class B: This class includes the 3-acylamino-thiophene-2-carboxamides **15, 26, 27** and the 5-aryl-3-acylamino-thiophene-2-carboxamides **16-18** (aryl group is 3-thiophenyl, phenyl and p-chlorophenyl respectively). Compound **14**, being a 3-amino-thiophene-2-carboxamide derivative is also included in class B. Derivatives **16** and **17** bind to $A_1/A_{2A}/A_3AR$ (K_i values 1.18, 4.69, 1.65 μM and 1.09, 7.29, 0.918 μM respectively). In **18** the 3-acylamino group is bulky and thus selectivity for A_3AR was obtained (K_i = 1.55 μM), while **15** which lacks 5-aryl substituent devoids of $A_{2A}AR$ affinity. In particular **15** exhibited an A_1/A_3AR affinity (K_i values 7.48 and 5.39 μM), along with **26** (K_i values 7.33 and 27.4 μM). Compound **27** demonstrated affinity against A_1 (K_i = 18 μM). In **14**, the lipophilic acyl substituent is not linked to the 3-amino group leading to moderate A_3AR affinity (K_i = 19.7 μM) and weak A_{2A} affinity (K_i = 31.7 μM), while the A_1 affinity was abolished.

Class C: This class includes methanimidothioate derivatives **2** and **19**. Compound **19** lacks any affinity compared to derivative **2** which exhibited moderate A_3AR affinity and a very weak $A_{2A}AR$ affinity (K_i values were 16.6 and 61.3 μM respectively). It seems that the substitution pattern is important for the affinity profile and this may trigger additional SAR studies in the future.

Class D: Members of this class are compounds **3, 5, 20-25** which bear a carbonyloxycarboximidamide segment, and **4** which bears a ureacarboximidamide. In most of the Class D compounds the carbonyl group of this fragment is connected to a 3-phenyl-isoxazole (a biaryl group) at 4-position and the carboximidamide carbon is connected to an aromatic moiety, like a substituted phenyl, pyridinyl or 4-thiazolyl group. The carbonyloxycarboximidamide derivatives **20, 22, 24** and **25** exhibited selective binding to A_3AR (from moderate to low micromolar affinity with K_i values being 30.9, 4.49, 4.16 and 0.899 μM). Compared to **20** the presence of the bulky iodine in the phenyl group in **21** led to increase in A_1/A_3AR affinity (K_i values 6.90 μM / 4.13 μM in **21** compared to > 100 μM / 30.0 μM respectively in **20**). Considering the structures of **5, 24**, and **25** possessing 2-methyl-1,3-thiazole linked to the carboximidamide carbon, the presence of a chloro substituent in the phenyl ring of 3-phenyl-isoxazole favors A_3AR selectivity. The measured K_i values of **5** were 21.8 / 9.45 μM for A_{2A}/A_3AR while **24** and **25** exhibited A_3AR selectivity with K_i values of 4.16 and 0.899 μM respectively. The transposition of the pyridinyl nitrogen from 3-position in **22** to 4-position in **23** effects a small decrease to A_3AR affinity, with a change of K_i value from 4.49 to 5.15 μM, and the appearance of a weak A_2AR affinity with K_i value of 30 μM. In the inactive derivative **3**, the monoaryl and biaryl groups are connected to the carbonyloxycarboximidamide fragment in a transposed way. In the inactive aminomethylidenehydrazine-1-carboxamide analogue **4** the carboxy group has been

replaced by an urea fragment.

Class E: This class contains molecules than cannot be classified in any of the above classes. The pyrimidin-4-amine **8** showed no AR binding. The ethyl 3-amino-1-acyl-1H-pyrazole-4-carboxylate **7** bound only to A_3AR with a $K_i = 18.3\ \mu M$. Compound **6** is an urea derivative with a weak affinity against A_3AR ($K_i = 30.6\ \mu M$).

Novelty of the tested ligands

The chemical novelty of the compounds was assessed based on their two-dimensional similarity to any known compound tested for binding to ARs. [17,18,19,20,21,22,23,24,25,28] Thus, we calculated the pairwise Tanimoto similarity, with extended chemical fingerprints for four atoms (ECFP4), for each of the compounds **1-27** to the thousands of known AR ligands in the ChEMBL22 [93,94] database using the Schrödinger Canvas program (radial fingerprints). [92] For each of the ligands **1-27**, the highest T_c value compared to all previously characterized AR ligands is presented in Table 1. A T_c value close to zero suggests no chemical similarity between a pair of molecules, whereas a value equal to one represents two identical molecules. Novel chemotypes for the ARs were discovered as reflected by their low Tanimoto coefficients ($T_c = 0.14$-0.33).

The 2-amino-3-aroylthiophenes [100,101,102,103,75,104,105] and the 2-amino-3-aroyl-5,6,7,8-tetrahydro-4H-cyclohepta[b]thiophenes, [105] which are respectively A_1AR allosteric agonists and A_1AR antagonists, [105,106] were found to be most similar with the A_{2A}/A_3AR ligands of class A ($T_c = 0.22$-0.34). Compounds of class B and D differ the most from previously known structures with $T_c < 0.17$ (see Tables 1, S4, and Supporting Information for the structures of the most similar compounds found for classes B-E). The results indicate that many compounds which are identified in the present study have not experimentally confirmed as binders to the relevant AR subtypes until now.

In two recent excellent studies, a detailed analysis of PAINS (pan-assay interference compounds) alerts [107] in compound libraries was performed. [108,109] From the analysis, it was concluded that the blind use of PAINS filters to detect compounds with possible PAINS liabilities should be handled with caution, since there is a trend to exclude *a priori* any potentially reactive compound from further consideration. In one of these studies [109] more than 14400 extensively tested compounds containing PAINS substructures were detected, and their hit rates were determined. After examining hundreds of assays, the hit frequency for PAINS was low, with values of two to five hits for PAINS, and many consistently inactive compounds were identified. Future investigations and certain well designed computational tools will be highly encouraged to translate the findings of rigorous large-scale data

analysis into practical guidelines with utility for medicinal chemistry. In these studies, 2-aminothiophenes were tested in about 650 assays and never produced a hit for PAINS. [109] Additionally, while in the original study, 2-amino-3-carbonylthiophenes [107] were suspected to be PAINS, extensive SAR studies showed that these compounds are promising allosteric A_1AR modulators. [103,75] Class A compounds **1**, **9-13** of the present study included a 2-aminothiophene scaffold. Compounds **5** and **20-25** included the carbonyloxycarboximidamide moiety which is not uncommon structural feature in medicinal chemistry projects. [110] We tested the studied compounds, encoded in smiles format, and none of the compounds was identified as PAINS. [111] Additionally, the model used to fit the binding data and determine K_i values of all compounds **1-27** confirms competitive interaction with the receptor and not a PAINS behavior. [99] Representative plots for compounds are shown in Figure 8. The results here show clearly specific and A_3-selective binding for a number of compounds. The fact that compound **25** and several other compounds show only A_3AR binding should serve as a valid proof of specific binding rather than random nonspecific interaction. Screening against other GPCRs would not provide a better control than the adenosine receptor subfamily for a possible PAINS behavior of the tested compounds.

Computational investigation of ligand-AR complexes

Common structural features in the tested compounds of the different classes A-E and in the receptor site among the different AR subtypes gave rise to similar contacts with residues of the binding area. Indeed, tested the 27 molecules resulted in similar, stable docking poses with a plausible profile as regarding the polar and lipophilic contacts inside the orthosteric binding area of A_1, A_{2A}, A_3 and $A_{2B}ARs$ (see for examples docking poses in Figures 1-7 and Figures S8-S14). It has been described how difficult it might be to select a proper binding conformation by taking into account only the docking score or the presence/absence of specific ligand receptor contacts. [40] An elaborate docking protocol was published which enabled a ligand-guided receptor optimization for the generation of conformational models for AR subtypes that effectively explain binding modes and subtype selectivity for a diverse set of known AR antagonists. [70]

The docking poses of the 27 ligands depicted in Table 1 in complex with A_1, A_{2A}, A_{2B}, and A_3ARs were inserted into a hydrated POPE lipid bilayer and MD simulations were performed on these systems. POPE membranes were preferred for the MD simulations over DMPC or POPC membranes after running MD simulations for 70 ns of the ZM241385-A_{2A} complex in the different hydrated lipid

bilayers and measuring ligand displacement, $RMSD_{lig}$, from its crystallographic coordinates. The smallest $RMSD_{lig}$ was measured with POPE, ensuring that MD simulations described well the stability of the ligand inside the orthosteric binding area (see Figures S4, S5). To establish that the comparison was meaningful, the equilibration of the membranes was also tested. To this end, the average area per lipid headgroup [81] was measured in the end of the simulation trajectory of each lipid and compared with experimental results. The calculated values approached the experimental ones for pure lipid bilayers only in the case of POPE (see Figure S6 and Table S2).

Changes in vdW interactions due to variations of the structure of the ligand structure and of the orthosteric binding site (see Figures 1-3) may result in significant changes of hydrogen bonding and the overall strength of the binding interactions. Firstly, the MD simulations of the complexes showed whether the ligand remained or escaped from the orthosteric binding area. To quantify this, the RMSD of the ligand was measured in respect to its docking pose coordinates (see $RMSD_{lig.}$ values in Table S3). For complexes where the ligand escapes from the orthosteric binding area, abolishing the combination of stabilizing H-bonding and van der Waals interactions, the $RMSD_{lig.}$ values were in most of the cases ≥ 4 Å. In those cases where the ligand retained a binding orientation similar to the starting docking pose the $RMSD_{lig.}$ values were < 3 Å. It was observed that the former complexes correspond to the inactive compounds ($K_i > 50$ μM; see in Table 1) and the latter complexes to compounds with a statistically significant experimental binding affinity ($K_i \leq 30$ μM; see in Table 1). We also selected a set of three ligands each being selective against A_1AR (coll6), $A_{2A}AR$ (ZM241385) and A_3AR (jaco_psb11) found in ref. 70. After docking using Gold against these AR subtypes, it was found that these compounds also docked well inside the binding area of every AR. The MD simulations resulted in a binding orientation similar to the docking pose, only for the AR to which the ligand is selective ($RMSD_{lig} < 1.5$ Å) while in any other case the ligand escaped from the binding area ($RMSD_{lig} \geq 4$ Å) (see Table S3 and Figures S11-S13). Similarly, compounds ZINC23192718, ZINC61843566, and ZINC18155583, which are decoys for $A_{2A}AR$, produced plausible docking poses but during the short MD simulation the ligands escaped from the $A_{2A}AR$ binding area. However, when bara_4p or veld_7 in ref. 70 were tested for their binding to A_1, A_{2A} and A_3 it was found that they docked well inside the binding area of the different ARs and that binding orientation of the starting docking pose was retained during the MD simulations for all the complexes despite the fact that bara_4p was A_3 selective and veld_7 was A_1 selective (Figure S14 and Table S3).

As illustrated above, if a ligand is observed to stay bound inside the binding site through MD simulations, it still may not be potent because its interactions still are not sufficiently favorable. A ligand which escapes from the binding area devoids of biological potency. A potent ligand always

adopts a stable binding orientation. This exact behavior was observed during the MD simulations of the particular set of ligands used in this work. The results of the procedure followed in this work which is based on $RMSD_{lig}$ were consistent with binding behavior of the compounds **1-27**. This procedure is not suggested as generally applicable to predict or explain potency to other systems. The in silico quantitative assessment of the experimental binding affinities needs the application of computational free energy methods. It is known that approximate free energy methods like MM-PBSA can provide good accuracy regarding the correlation between calculated ΔG_{bind} and experimental pK_i values for K_i's covering a range of 10^3 corresponding to a $\Delta\Delta G_{bind}$ scale equal to 4-5 kcal mol^{-1}. [112, 113, 36, 31] In the present work, a K_i of 50 μM corresponds to an almost inactive compound compared to an active one having for example a K_i = 5 μM . Such two compounds differ in ΔG_{bind} by 1.5 kcal mol^{-1}, which is well below the accuracy of the MM-PBSA method. In order to explain smaller differences in affinity (as for example between compounds **24** and **25**), more accurate free energy methods are needed. [114] Our group has previously applied such methods for this narrow range of binding free energies with success [115] [116] but this approach is beyond the aim of the present work.

Secondly, the MD simulations were performed to investigate the binding interactions with A_1, A_{2A}, and A_3ARs for compounds exhibiting affinity. Important changes and SAR results for the most significant molecules among **1-27**, included in classes A, B and D, are discussed.

Class A: Compounds **1**, **12** and **13** contain one bulky lipophilic CONH-N=CH-Ar group and one phenyl group respectively linked at 3- and 5-positions of the 2-aminothiophene ring. Similarly, ZM241385 contains one $NH(CH_2)_2Ph(OH)$ fragment and one 2-furyl group respectively linked to 5- and 2-positions respectively of a bicyclic 7-aminotriazolotriazine. The docking calculations and 100 ns MD simulations showed that **1**, **12** and **13** are stabilized inside the binding pocket of $A_{2A}AR$ with similar orientation to ZM241385 (Figures 1a,b and S1) resulting in good affinity against $A_{2A}AR$ (K_i = 2.67, 3.93 and 4.59 μM respectively). The 2-amino group of the thiophene ring is hydrogen-bonded to the side chain carbonyl of N(6.55) and to the carboxylate group of E(5.30) in EL2 (see panel b in Figure 1 for compound **13**). The thiophene ring participates in an aromatic π-π stacking interaction with the conserved F(5.29) (EL2) and forms important hydrophobic contacts with I(7.39) (Figure 1a) while sulfur atom forms H-bonds with the side chain amide group of N(6.55) (Figure 1b). The CONH-N=CH-Ar moiety is oriented towards the solvent-exposed part of the binding cavity [15] (EL2 and EL3) or at the extracellular end of TM2, between TM1 and TM7 and forms hydrophobic interactions with L(7.32) and M(7.35) (Figure 1a). [15,16] This is a similar orientation of the $(CH_2)_2Ph(OH)$ fragment found in the two X-ray structures of A_{2A}-ZM241385 (see Figure 1b and Figures S1-S3). [15,16] Thus in the extracellular end of the receptor, a tremendous flexibility of the ligand is observed compared to

that of the TM domain. The 5-phenyl group is positioned deeply inside the ligand-binding cavity towards TM5 and TM7, engaging in hydrophobic interactions with V(3.32), L(3.33), L(6.51), H(6.52), and W(6.48) (Figure 1a,b). In ZM241385, a furyl group forms hydrophobic interactions with these residues and is also hydrogen bonding to the side chain amido group of N(6.55); this ring has been implicated in both antagonist and agonist binding, as revealed by mutagenesis experiments. [117,118]

The other members of this class, compounds **9-11**, lack affinity due to the absence of important attractive interactions or exert repulsive forces inside the binding area. Thus, in **9,** the 5-phenyl group is missing and according to the calculations, the ligand cannot form additional attractive van der Waals interactions with residues V(3.32), L(3.33), L(6.51), and H(6.52) positioned deeper in the orthosteric binding area compared to compounds **1, 12** and **13**. The docking calculations suggested that in **10** and **11** the condensed cyclopentane or cyclohexane ring exerts steric repulsion to the phenyl group of F(5.29) resulting in the abolishment of the critical H-bonding interactions with N(6.55), which was confirmed by the MD trajectories before even reaching 10 ns (Figure 4a).

The docking calculations showed that compounds **1**, **9-13** bind inside A_1AR with similar interaction patterns, but the MD simulation trajectories revealed that the binding poses of **1**, **9-12** were not stable before reaching 10 ns (Figure 4a). The 100 ns MD simulation revealed a stable binding orientation for **13** inside A_1AR. Indeed, with the exception of **13** ($K_i = 15.2\ \mu M$) (Figure 2a,b), none of the other ligands in this class (**1** and **9-12**) exhibited affinity against A_1AR. If we compare the residues in the orthosteric binding area of the ARs, the A_1 subtype has the highest homology to A_{2A} with only four side chain substitutions on the periphery of the binding pocket. The binding area similarity between A_1 and $A_{2A}ARs$ is 80% while A_3 and $A_{2A}AR$ showed 53.33% sequence similarity in the binding area (Figure S7). However, the shape of the binding area differs from $A_{2A}AR$ according to the recently published X-ray structure of A_1AR in complex with the covalently bound antagonist DU172. [32] It was shown that the A_2AR binding pocket is elongated and narrow compared to the very wide and open cavity of the A_1AR due to the movements of TM1,2,3 and 7, along with EL3. The A_2AR pocket is narrower since M(7.35) acts as a gatekeeper (see Figure 1a) preventing entry and binding of bulky substituents. There is a common region covered by ZM241385 inside $A_{2A}AR$ and DU172 inside A_1AR, despite their different orientation and depth inside the cavity, and different the shapes and volumes of the binding area. The key interactions anchoring ligands ZM241385 and DU172 with their respective receptor subtype are preserved. These include a π-π stacking interaction with F(5.29) and a bidentate hydrogen bond with N(6.55) formed by different groups linked with the xanthine ring of DU172 and the triazolotriazine ring of ZM241385. It was suggested [32] that the binding area of A_1AR includes the orthosteric and a secondary allosteric binding pocket - the latter not being present in

A$_{2A}$AR. When less bulky orthosteric antagonists than DU172, such as DPCPX, are docked into the A$_1$AR, a significant part of the binding site is left un-accommodated. This is shown in Figures 1a and 2a for compound **13** occupying the orthosteric binding area inside A$_{2A}$ and A$_1$ARs with the CONH-N=CH-Ar moiety orienting towards the solvent-exposed part of the open binding cavity. [15] Compared to A$_{2A}$AR complex, **13** inside the A$_1$AR was positioned closer to TM5 and TM6. This may be the result of the more polar environment at the extracellular opening of the A$_1$AR pocket compared to A$_{2A}$AR. The more polar environment is attributed to the presence of T(7.35) instead of M and the mutations L(5.28)E and L(7.32)S, combined with a slight shift in the conformation of E(5.30) (Figure 2a,b). This polar environment may limit the presence of bulky lipophilic groups in the area between EL2 and TM7, disfavoring a stable orientation where the hydrogen bonding interactions with N(6.55) and E(5.30) of the relevant ligands take place. Thus, among compounds **1**, **12**, and **13**, only the third, possessing an Ar = Ph in CONH-N=CH-Ar moiety, binds to A$_1$AR (Figures 1, 2) in contrast to **1** and **12** where the phenyl ring is substituted with one or three methoxy groups respectively (see Figure 5 for **1**). Regarding compounds **9**, **10** and **11**, the MD simulations suggested that no stable complex is formed at the orthosteric binding region of A$_1$AR (see Figure 4b for ligand **11**), similarly to the case with A$_{2A}$AR described above.

All molecules **1**, **9-13** exert moderate weak to low micromolar affinity against A$_3$AR with K_i values of 37.1, 16.5, 14.8, 5.77, 5.16 and 3.10 μM respectively. At the 5.30 position of A$_3$AR subtype unlike the A$_{2AR}$, the glutamic acid is substituted with valine. As a consequence, ligands with lipophilic groups can be accommodated more effectively in this region of the binding area compared to the other AR subtypes (Figure 3a,b). These bulky groups are tolerated since V(5.30) can produce suitable rotamers which enable the reduction of van der Waals repulsions. [15,70] Similarly, the replacements T(6.58)I, M(7.35)L allow the presence of bulky groups to protrude towards the extracellular opening of the pocket (see Figure 3b). It was shown [70] that when an optimized conformation of V(5.30) side chain was applied in control docking calculations against A$_3$AR, the enrichment of known A$_3$AR ligands with bulky amine substitutions or neighboring lipophilic fragments among a database of decoys was substantially increased. Hence, we adopted this rotamer and obtained reliable binding poses in which the CONH(CH$_2$)$_2$Ar moiety in **9-11** and the CONH-N=CH-Ar moiety in **12** and **13** were oriented towards the solvent-exposed part of the open binding cavity (Figures 3a,b, 4c, 5c). The molecules shifted slightly towards TM5 and TM6, compared to their binding orientations against A$_{2A}$ and A$_1$ARs, to fit better their bulky lipophilic groups close to V(5.30). The 100 ns MD simulations showed that the binding orientation of compound **13** was stabilized through the hydrogen bonding of the 2-amido group of the ligand with the side chain carbonyl group of N(6.55) and equally with the

carbonyl group of F(5.43) or S(6.53) of the TM helices; in this last case, the NHCO group of the ligand interacted with N(6.55) (see Figure 3a,b). Furthermore, H-bonding interactions between N(6.55) amide side chains and the sulfur atom of the thiophene ring of the ligand were observed in the trajectory. Compounds **9-11** were less potent compared to **1**, **12** and **13**. Compound **9** lacks a 5-phenyl group which may allow attractive interactions with residues L(6.51) and H(6.52) deeply inside the binding area; the 5-aryl group seems to be favorable for binding to A_1 and A_{2A}ARs according to the results of the present study. As discussed previously for **10** and **11**, the condensed cyclopentane and cyclohexane ring prevents the ligand from adopting an optimal orientation for H-bonding interactions with N(6.55). Nevertheless, these molecules fit inside the more lipophilic binding area of A_3AR, according to the MD simulations for 100 ns, in contrast to A_1 and A_{2A}ARs (Figure 4). Between **1**, **12** and **13** the most potent ligand against A_3AR is **1**, in agreement with the more favorable interactions in the region around V(5.30) due to presence of a more lipophilic group (Figure 3a,b, 5c). Compound **13** was found to bind to A_1, A_{2A} and A_3AR.

Class B: Similarly to what was discussed for **13**, the docking calculations and MD simulations against A_{2A} and A_1ARs showed that the bulky lipophilic groups of **16**, **17** are likewise oriented to the area of EL2 (Figure 6, Figure S8). The measured affinity of **16**, **17** measured against A_{2A}AR was $K_i =$ 1.18, 1.09 μM and against A_1AR was 4.69 and 7.29 μM, respectively. Similarly to the 2-amino group binding to N(6.55) in class A molecules, the 100 ns MD simulations showed that the 2-amido group of the thiophene ring can be hydrogen-bonded to the amido group of N(6.55) in A_{2A} and A_1AR and/or with the carboxylate group of E(5.30), while sulfur of the thiophene ring may also form a H-bond with the amido group of N(6.55). The 100 ns MD simulations showed that the van der Waals interactions of **16** and **17** inside the binding cavity of A_{2A}AR are similar to those described above for the A_{2A} in complex with **13** of class A molecules. The 100 ns MD simulation of the A_1AR-**17** complex showed that the ligand moved slightly higher in the orthosteric binding site and the 5-aryl-thiophene ring was inclined so that the 3-NHCOR substituent can be directed between TM7 and TM2, compared to A_{2A}-AR-**17** complex. The 2-amido carbonyl group of the ligand can be hydrogen-bonded to E(5.30). This movement can be realized due to the broader area between TM1, TM2,TM5 and TM6 as it was shown recently in the X-ray structure of the A_1AR-DU172 complex (PDB ID 5UEN [32]). The ligand is embraced by Y(7.36), H(7.43), L(7.32), L(6.51), F(5.29), L(5.28) and I(2.66), and the thiophene ring induces an aromatic π-π stacking interaction with F(5.29) (Figures 6, S7). This orientation cannot be adopted by **16**, possibly because of its longer 3-NHCOR group. The 100 ns MD simulations showed that in this case the entire molecule shifts slightly towards TM2. The 2-amido carbonyl group of the ligand can be hydrogen-bonded to the side chain of N(6.55), while the amino part of that same group

to the carboxylate of E(5.30). The NH part of the 3-NHCOR moiety can be also hydrogen-bonded to E(5.30) side chain. The replacement of E(5.30) with V in A$_3$AR orthosteric cavity retained the binding of compounds **16** and **17** as shown by their respective K_i values of 1.65 and 0.918 μM, with the latter value corresponding to one of the lowest affinities against A$_3$AR. The 100 ns MD simulations showed that the molecules shifted slightly towards TM5 and TM6, compared to their binding orientations against A$_{2A}$ and A$_1$ARs, to fit better their bulky lipophilic groups close to V(5.30) (Figure 6). The ligands were stabilized through the formation of a bidentate hydrogen bond between their 2-amido group and the amide side chain of N(6.55).

In compound **18**, the thiophene ring possesses a NHCOCH$_2$SPh(CF$_3$)$_2$ moiety. The MD simulations predicted that **18** cannot be stabilized inside the orthosteric binding area of A$_{2A}$ and A$_1$ARs, either when NHCOR group is oriented towards the solvent exposed area - because of the presence of two polar CF$_3$ groups in the area close to E(5.30) - or when NHCOR group is oriented towards TM2 - since the group is bulky and the molecule should anchor the p-Cl-phenyl group in the receptor. In contrast, an orientation of NHCOCH$_2$SPh(CF$_3$)$_2$ moiety pointing to the solvent-exposed area was well accommodated by the replacement of E(5.30) with V and the 100 ns MD simulation trajectory revealed a stable complex. Indeed compound **18** was the only class B antagonist with affinity solely against A$_3$AR (K_i = 1.55 μM). Compared to **16-18**, compounds **15**, **26** and **27** lack the 5-phenyl substituent, which led to affinity only against A$_1$ and A$_3$AR for **15**, **26** or A$_1$ for **27** (K_i = 7.48, 5.39 μM for **15**, K_i = 7.33, 27.4 μM for **26** and K_i = 18 μM for **27**). The results showed that a substituent buried deep between TM3, TM5, TM6 and TM7, and making contacts with V(3.32), L(3.33), L(6.51), and H(6.52) is important for affinity against A$_{2A}$R, similarly to the 2-furyl substituent of ZM241385 as has been demonstrated from antagonist and agonist binding and mutagenesis experiments. [117,118] Compound **14** which lacks the bulky 3-acylamino substituent of the 3-thiophene ring (compare to structures of **16** and **17**) has a moderate affinity against A$_{2A}$ and A$_3$ARs and no affinity against A$_1$AR.

Class D: These molecules have a propensity to exhibit selectivity for A$_3$AR. The docking poses and the 100 ns MD simulations showed that the bulky phenyl-isoxazole biaryl group can be positioned close to V(5.30) of the A$_3$AR orthosteric binding area. In this binding position the phenyl group of the 3-phenyl-isoxazole can interact -through attractive van der Waals forces- with the iPr side chain of Val, and the isoxazole ring can engage in an aromatic π-π stacking interaction with the phenyl group of F(5.29) (Figures 7, S15, S16). The monoaryl group is oriented deeper into the receptor favouring interactions with L(6.51). The binding orientation is stabilized due to the H-bonding interactions between: a) the amino group of the carbonyloxycarboximidamide molecular segment and the amide

sidechain of N(6.55) along with the backbone carbonyl of L(6.51). b) the nitrogen and oxygen atoms of isoxazole and the NH groups of F(5.29) and V(5.30), respectively. c) the thiazole monoaryl group N or S and N(6.55) sidechain. Compounds **22**, **24** and **25** were selective against A$_3$AR with K_i values 4.49, 4.16 and 0.899 μM respectively. Compound **21** binds also to A$_1$AR and **23** and **5** bind also to A$_{2A}$AR. Compound **21** shows a K_i = 6.90 μM for A$_1$AR and 4.13 μM for A$_3$AR. Compound **23** shows K_i = 30 μM for A$_{2A}$AR and 5.15 μM for A$_3$AR. Compound **5** shows a K_i = 21.8 μM for A$_{2A}$AR and 9.45 μM for A$_3$AR. When the residue (5.30) is changed from valine to the negative charged glutamic acid in A$_{2A}$AR, the phenyl group of 3-phenyl-isoxazole can be oriented towards the TM2 through rotation around the biaryl-carbonyloxy bond to avoid any unfavourable interactions with the E(5.30) carboxylate group. Representative MD simulations of **5** showed that this movement enabled the ligand to be stabilized inside the A$_{2A}$AR orthosteric binding area between TM5, TM6 and TM2 with the monoaryl group being in spatial vicinity to TM5 and the phenyl-isoxazolyl group close to TM2. This region is wider, and thus the ligand cannot bind tightly inside A$_1$AR (Figure 7). Compared to **5**, compound **25** possesses two chlorine atoms attached to the phenyl ring and this resulted in the selectivity of **25** against A$_3$AR. The MD simulations showed that the dichlorophenyl ring favors increased van der Waals interactions with F(5.29) and V(5.30) which enable the ligand to form stronger H-bonding interactions with side chain of N(6.55) and the backbone carbonyl of L(6.51) (see the ligand-protein diagrams in Figures S15, S16). In **3**, which lacks affinity for all ARs, the monoaryl and biaryl groups are connected to the carbonyloxycarboximidamide fragment in a transposed manner, i.e. the biaryl group is connected to the carboximidamide carbon and the monoraryl moiety to the carbonyl group. The biaryl group is bulky and cannot be fitted deep into the receptor, towards L(6.51) and W(6.48). This kind of transposition in N-acylhydrazones [119] has previously shown to affect seriously the affinity for A$_{2A}$AR. In the aminomethylidenehydrazine-1-carboxamide **4**, some proximal polar groups are simultaneously present, i.e. the methylidenehydrazide group, the urea group and pyridine. All of these groups provide H-bond donor atoms which are in spatial proximity, thus interacting at the same space, prohibiting the stabilizing binding to N(6.55) or/and E(5.30). Indeed, the molecule was not stable inside the binding area, according to the MD simulations.

MD simulations were also performed for compounds of Classes C and E (see Figure S9; relevant information for these compounds can be found in the Supporting Information). The MD simulations for some A$_{2B}$-ligand complexes showed that the ligand retained a binding orientation similar to the starting docking pose after 100 ns (see Figure S10). Since all compounds were inactive against A$_{2B}$AR, according to an adenylyl cyclase activity assay, [120] the simulation results were deemed ambiguous and no additional simulations were realized. Most likely, a different experimental structure of the binding

area exists that deviates from that predicted by homology modeling.

Conclusions

Pharmaceutical companies and academic research laboratories are involved in intense efforts to identify antagonists with selectivity for each adenosine receptor (AR) subtype as potential clinical candidates for "soft" treatment of different diseases. $A_{2A}R$ antagonists can be useful for treating cancer, central nervous system (CNS) disorders; A_1AR antagonists can provide kidney-protective agents, anti-asthmatic and CNS agents; A_3AR antagonists are promising for therapeutic applications in asthma, glaucoma and $A_{2B}AR$ antagonists for diabetes, asthma and chronic obstructive pulmonary disease.

The reported crystal structures of $A_{2A}AR$ in complex with agonists or antagonists [15,16,21,121,122,123] and of A_1AR with an antagonist, [32,33] along with other advances attributed to the progress of GPCR crystallography [124] have made structure-based approaches an attractive strategy for drug design against adenosine receptors which are pharmaceutically important targets. The $A_{2A}AR$ is one of the best studied receptors of all class A GPCRs. Additionally, among the 688 known GPCRs, class A is the 7th more intensely investigated. The application of virtual screening and medicinal chemistry studies for a few decades now has resulted in a high number of bioactive compounds (~ 11000) against $A_{2A}AR$ as was retrieved from ChEMBL20. In the present study, we performed virtual screening of a small Maybridge library of 14400 compounds for $A_{2A}AR$, using its crystallographic structure in complex with the antagonist ZM241385, through a combination of structure-based and ligand-based procedures. After docking, the ligand poses were re-scored by applying CHARMM energy minimization and consideration of desolvation energy electrostatics using the Poisson-Boltzmann equation. Out of the eight selected and tested compounds, three showed micromolar affinity for the A_{2A} and A_3ARs and two were low micromolar binders only to the A_3AR receptor. Thus, although initially targeting the A_2AR, the project resulted in the following percent of successful antagonist hits: 25% for A_{2A} and 63% for A_3AR. In a second step, based on the structure of mainly two promising active hits, possessing a 2-amino-thiophene-3-carboxamide and a carbonyloxycarboximidamide chemotype respectively, 19 more compounds were selected by similarity for testing. For this second series of seventeen compounds, sixteen were found to bind to the ARs family. Eight of those revealed A_3-selective affinity with K_i values in the micromolar to low micromolar regime.

The 27 tested molecules resulted in similar docking poses against A_1, A_{2A}, A_{2B} or A_3ARs. The MD simulations of numerous complexes using Desmond/OLPS2005 and Amber/ff14sb provided the

basic features of the binding interactions with A_1, A_{2A}, and A_3ARs for compounds exhibiting affinity. Using the docking poses of the antagonists as starting structures, the MD simulations suggested features of their binding inside the orthosteric binding area of A_{2A}, A_1 and A_3ARs. The complexes with A_{2A} and A_1ARs were stabilized through H-bonding interactions between an amino or amido group of the ligand and N(6.55) of the AR. E(5.30) can be involved also in H-bonding interactions with the bound ligand. A_{2A}AR antagonists include a lipophilic bulky substituent which was oriented towards the extracellular area, close to EL2 and TM7, and a smaller lipophilic group which was fitted deep in the binding region, close to L(6.51) and H(6.52). Similar interactions were described in the X-ray structures between antagonists and A_{2A}AR. [15,16,21] Interestingly, for the A_1AR antagonists the ligand covers a larger space between TM5/TM6 and TM1/TM2, as shown in the recent X-ray structure between an antagonist and A_1AR. [32] Many of the ligands studied in this report may be considered to be more lipophilic than ZM241385 (which has a triazolotriazine central ring) and it was found that most of them (**1, 2, 5-7**, **9-18** and **20-25**) interact with A_3AR. We suggest that selectivity against A_3AR is boosted by increasing the size and lipophilicity of a suitable substituent reflecting a better fit with V(5.30). Compounds **6**, **7**, **9-11**, **18**, **20**, and **22-25** acted as selective antagonists against A_3AR. These findings are in line with the previously published results on highly selective A_3AR agonists and antagonists with a bulky group in a compatible position, e.g. the introduction of a 3-iodo-benzyl group in N^6 position in 2-Chloro-N^6-(3-iodobenzyl)-adenosine-5′-N-methyluronamide (Cl-IB-MECA) increases the affinity of this adenosine derivative for A_3AR.[118,119]

Relatively novel chemotypes of ARs antagonists were identified. Two classes of compounds were found with low T_c values (< 0.17): a) The 3-acylamino-5-aryl-thiophene-2-carboxamides (class B) including the new substitution pattern (2-$CONH_2$ and 3-NHCOR) of the thiophene ring, which - compared to 2-NH_2 and 3-CONHR' substitution pattern- enhanced the affinity for A_1 and A_3AR. b) The carbonyloxycarboximidamide derivatives (class D), which favour A_3AR affinity. The A_3AR subtype is the most divergent from all other ARs, with 10 out of 20 side chains in the binding pocket being unique. The micromolar affinity, selective A_3AR antagonists found here provide novel, relatively simple chemotypes which may contribute to the treatment of the A_3AR-related human pathologies.

We consider these findings to be an important contribution to the field of structure-based drug design against ARs and also a valuable example showing that the *in silico* screening of a small library against a receptor family can lead to novel hits when careful scoring of the relative free energy of binding is applied.

6 Supporting Information available

Supplementary material includes fourteen figures, details and results from few complementary MD simulations and five tables. This material is available free of charge *via* the Internet at http://pubs.acs.org.

7 Acknowledgements

8 Author Information

[*] Corresponding author: Antonios Kolocouris (A.K.), Panepistimioupolis – Zografou, 15771 Athens, Greece; Phone: (+301) 210-7274834, Fax: (+301) 210 727 4747; E-mail: ankol@pharm.uoa.gr

A.K. designed this research project. A.K. performed the docking calculations for VS with different scoring functions and calculations with CHARMM; M.C. helped towards that aim. G.O. performed some docking calculations at the early stages of the project. P.L. in A.K. group performed homology modelling, docking calculations, numerous MD simulations and similarity calculations as part of his

Ph.D work and E.V. helped towards that aim. D.S. did the computational work for compounds **26**, **27**. P.L. and G.L. performed MD simulations using Amber. K.-N.K group did the biological evaluation. A.K. wrote the manuscript assigning contributions of all the authors; T.M aided in the improvement of the revised version; M.C., T.M.; E.V., D.S., K.-N.K, and G.O. revised it.

9 Abbreviations

Transmembrane, TM; Extracellular loop, EL2; POPE, 1-palmitoyl-2-oleoyl-*sn*-glycero-3-phosphoethanolamine; POPC, 1-palmitoyl-2-oleoyl-*sn*-glycero-3-phosphocholine; GPCRs, G protein-coupled receptors; MD, Molecular dynamics; CNS, central nervous system; PD, Parkinson's disease; RMSD, root-mean-square deviation; PB, Poisson-Boltzmann; PDB, Protein data bank; OPM, Orientations of Proteins in Membranes; PME, particle mesh Ewald method; RESPA, Reversible multiple time scale molecular dynamics; ROCS, Rapid Overlay of Chemical Structures; ECFP4, extended chemical fingerprints for four atoms; CheMBL, Cheminformatics European Molecular Biology Laboratory CCPA, 2-chloro-N6-cyclopentyladenosine; NECA, 5'-N-ethylcarboxamidoadenosine; HEMADO, 2-hexyn-1-yl-N^6-methyladenosine. DPCPX, Dipropylcyclopentylxanthine.

10 References and Notes

(1)   Fredholm, B. B.; IJzerman, A. P.; Jacobson, K. A; Klotz, K. N.; Linden, J. International Union of Pharmacology. XXV. Nomenclature and Classification of Adenosine Receptors. *Pharmacol. Rev.* **2001**, *53*, 527–552.

(2)   Fredholm, B. B.; Ijzerman, A. P.; Jacobson, K. A.; Linden, J.; Müller, C. E. International Union of Basic and Clinical Pharmacology. XXXI. Nomenclature and Classification of Adenosine Receptors — An Update. *Pharmacol. Rev* **2011**, *63*, 1–34.

(3)   Chen, J.-F.; Eltzschig, H. K.; Fredholm, B. B. Adenosine Receptors as Drug Targets--What Are the Challenges? *Nat. Rev. Drug Discov.* **2013**, *12*, 265–286.

(4)   Alnouri, M. W.; Jepards, S.; Casari, A.; Schiedel, A. C.; Hinz, S.; Müller, C. E. Selectivity Is Species-Dependent: Characterization of Standard Agonists and Antagonists at Human, Rat, and Mouse Adenosine Receptors. *Purinergic Signal.* **2015**, *11*, 389–407.

(5)   de Lera Ruiz, M.; Lim, Y.; Zheng, J. Adenosine A2A Receptor as a Drug Discovery Target. *J. Med. Chem.* **2014**, *57*, 3623–3650.

(6)   Flögel, U.; Burghoff, S.; Van Lent, P. L. E. M.; Temme, S.; Galbarz, L.; Ding, Z.; El-Tayeb, A.; Huels, S.; Bönner, F.; Borg, N.; Jacoby, C.; Müller, C. E.; Van Den Berg, W. B.; Schrader, J. Selective Activation of Adenosine A2A Receptors on Immune Cells by a CD73-Dependent Prodrug Suppresses Joint Inflammation in Experimental Rheumatoid Arthritis. *Sci. Transl. Med.* **2012**, *4*, 146ra108.

(7)   Stößel, A.; Schlenk, M.; Hinz, S.; Küppers, P.; Heer, J.; Gütschow, M.; Müller, C. E. Dual Targeting of Adenosine A2A Receptors and Monoamine Oxidase B by 4H-3,1-Benzothiazin-4-Ones. *J. Med. Chem.* **2013**, *56*, 4580–4596.

(8)   Gnad, T.; Scheibler, S.; Kugelgen, I. Von; Scheele, C.; Kilic, A.; Glode, A.; Hoffmann, L. S.; Reverte-Salisa, L.; Horn, P.; Mutlu, S.; El-Tayeb, A.; Kranz, M.; Deuther-Conrad, W.; Brust, P.; Lidell, M. E.; Betz, M. J.; Enerback, S.; Schrader, J.; Yegutkin, G. G.; Müller, C. E.; Pfeifer, A. Adenosine Activates Brown Adipose Tissue and Recruits Beige Adipocytes via A2A receptors. *Nature* **2014**, *516*, 395–399.

(9)   Fuentes, E.; Fuentes, M.; Caballero, J.; Palomo, I.; Hinz, S.; El-Tayeb, A.; Müller, C. E. Adenosine A2A Receptor Agonists with Potent Antiplatelet Activity. *Platelets* **2017**, *0*, 1–9.

(10)   Linden, J. New Insights into the Regulation of Inflammation by Adenosine. *J. Clin. Invest.* **2006**, *116*, 1835–1837.

(11)   Holgate, S. T. The Quintiles Prize Lecture 2004. The Identification of the Adenosine A2B Receptor as a Novel Therapeutic Target in Asthma. *Br. J. Pharmacol.* **2005**, *145*, 1009–1015.

(12)   Ortore, G.; Martinelli, A. A2B Receptor Ligands: Past, Present and Future Trends. *Curr. Top. Med. Chem.* **2010**, 923–940.

(13)   Schenone, S.; Brullo, C.; Musumeci, F.; Bruno, O.; Botta, M. A1 Receptors Ligands: Past, Present and Future Trends. *Curr. Top. Med. Chem.* **2010**, *10*, 878–901.

(14)   Borea, P. A.; Varani, K.; Vincenzi, F.; Baraldi, P. G.; Tabrizi, M. A.; Merighi, S.; Gessi, S.; Cacciari, B.; Romagnoli, R.; Merighi, S.; Varani, K.; Borea, P. A.; Spalluto, G. The A3 Adenosine Receptor: History and Perspectives. *Pharmacol. Rev.* **2015**, *67*, 74–102.

(15)   Jaakola, V.-P.; Griffith, M. T.; Hanson, M. A.; Cherezov, V.; Chien, E. Y. T.; Lane, J. R.; Ijzerman, A. P.; Stevens, R. C. The 2.6 Angstrom Crystal Structure of a Human A2A Adenosine Receptor Bound to an Antagonist. *Science* **2008**, *322*, 1211–1217.

(16)   Doré, A. S.; Robertson, N.; Errey, J. C.; Ng, I.; Hollenstein, K.; Tehan, B.; Hurrell, E.; Bennett,

K.; Congreve, M.; Magnani, F.; Tate, C. G.; Weir, M.; Marshall, F. H. Structure of the Adenosine A(2A) Receptor in Complex with ZM241385 and the Xanthines XAC and Caffeine. *Structure* **2011**, *19*, 1283–1293.

(17) Carlsson, J.; Yoo, L.; Gao, Z.; Irwin, J.; Shoichet, B.; Jacobson, K. Structure-Based Discovery of A(2A) Adenosine Receptor Ligands. *J. Med. Chem.* **2010**, *53*, 3748–3755.

(18) Katritch, V.; Jaakola, V.-P.; Lane, J. R.; Lin, J.; Ijzerman, A. P.; Yeager, M.; Kufareva, I.; Stevens, R. C.; Abagyan, R. Structure-Based Discovery of Novel Chemotypes for Adenosine A(2A) Receptor Antagonists. *J. Med. Chem.* **2010**, *53*, 1799–1809.

(19) Chen, D.; Ranganathan, A.; IJzerman, A. P.; Siegal, G.; Carlsson, J. Complementarity between in Silico and Biophysical Screening Approaches in Fragment-Based Lead Discovery against the A(2A) Adenosine Receptor. *J. Chem. Inf. Model.* **2013**, *53*, 2701–2714.

(20) van der Horst, E.; van der Pijl, R.; Mulder-Krieger, T.; Bender, A.; Ijzerman, A. P. Substructure-Based Virtual Screening for Adenosine A2A Receptor Ligands. *ChemMedChem* **2011**, *6*, 2302–2311.

(21) Congreve, M.; Andrews, S. P.; Dore, A. S.; Hollenstein, K.; Hurrell, E.; Langmead, C. J.; Mason, J. S.; Ng, I. W.; Tehan, B.; Zhukov, A.; Weir, M.; Marshall, F. H. Discovery of 1,2,4-Triazine Derivatives as Adenosine A(2A) Antagonists using Structure Based Drug Design. *J. Med. Chem.* **2012**, *55*, 1898–1903.

(22) Langmead, C. J.; Andrews, S. P.; Congreve, M.; Errey, J. C.; Hurrell, E.; Marshall, F. H.; Mason, J. S.; Richardson, C. M.; Robertson, N.; Zhukov, A.; Weir, M. Identification of Novel Adenosine A2A Receptor Antagonists by Virtual Screening. *J. Med. Chem.* 2012, *55*, 1904–1909.

(23) Rodríguez, D.; Gao, Z.-G.; Moss, S. M.; Jacobson, K. A.; Carlsson, J. Molecular Docking Screening Using Agonist-Bound GPCR Structures: Probing the A2A Adenosine Receptor. *J. Chem. Inf. Model.* **2015**, *55*, 550–563.

(24) Jazayeri, A.; Andrews, S. P.; Marshall, F. H. Structurally Enabled Discovery of Adenosine A_{2A} Receptor Antagonists. *Chem. Rev.* **2017**, 117, 21-37.

(25) Lenselink, E. B.; Beuming, T.; van Veen, C.; Massink, A.; Sherman, W.; van Vlijmen, H. W. T.; IJzerman, A. P. In Search of Novel Ligands Using a Structure-Based Approach: A Case Study on the Adenosine A2A Receptor. *J. Comput. Aided. Mol. Des.* **2016**, *30*, 863–874.

(26) Tian, S.; Wang, X.; Li, L.; Zhang, X.; Li, Y.; Zhu, F.; Hou, T.; Zhen, X. Discovery of Novel and Selective Adenosine A 2A Receptor Antagonists for Treating Parkinson's Disease through Comparative Structure-Based Virtual Screening. *J. Chem. Inf. Model.* **2017**, *57*, 1474-1487.

(27) Kolb, P.; Phan, K.; Gao, Z.-G.; Marko, A. C.; Sali, A.; Jacobson, K. a. Limits of Ligand Selectivity from Docking to Models: In Silico Screening for A(1) Adenosine Receptor Antagonists. *PLoS One* **2012**, *7*, e49910.

(28) Ranganathan, A.; Stoddart, L. A.; Hill, S. J.; Carlsson, J. Fragment-Based Discovery of Subtype-Selective Adenosine Receptor Ligands from Homology Models. *J. Med. Chem.* **2015**, *58*, 9578–9590.

(29) Kim, J.; Wess, J.; van Rhee, A. M.; Schöneberg, T.; Jacobson, K. A. Site-Directed Mutagenesis Identifies Residues Involved in Ligand Recognition in the Human A Adenosine Receptor. *J. Biol. Chem.* **1995**, *270*, 13987–13997.

(30) Gao, Z.; Chen, A.; Barak, D.; Kim, S.; Mu, C. E.; Jacobson, K. A. Identification by Site-Directed Mutagenesis of Residues Involved in Ligand Recognition and Activation of the Human A3 Adenosine Receptor. *J. Biol. Chem.* **2002**, *277*, 19056–19063.

(31) Ballesteros, J. A.; Weinstein, H. Integrated methods for the construction of three-dimensional models and computational probing of structurefunction relations in G protein coupled receptors. *Methods Neurosci.* **1995**, *25*, 366–428.

(32) Glukhova, A.; Thal, D. M.; Nguyen, A. T.; Vecchio, E. A.; Jörg, M.; Scammells, P. J.; May, L.

T.; Sexton, P. M.; Christopoulos, A. Structure of the Adenosine A_1 Receptor Reveals the Basis for Subtype Selectivity. *Cell* **2017**, *168*, 867–877.

(33) Cheng, R. K. Y.; Segala, E.; Robertson, N.; Deflorian, F.; Doré, A. S.; Errey, J. C.; Fiez-Vandal, C.; Marshall, F. H.; Cooke, R. M. Structures of Human A1 and A2A Adenosine Receptors with Xanthines Reveal Determinants of Selectivity. *Structure* **2017**, *25*, 1275–1285.

(34) Yuriev, E.; Ramsland, P. A. Latest Developments in Molecular Docking: 2010-2011 in Review. *J. Mol. Recognit.* **2013**, *26*, 215–239

(35) Kollman, P. A.; Massova, I.; Reyes, C.; Kuhn, B.; Huo, S.; Chong, L.; Lee, M.; Lee, T.; Duan, Y.; Wang, W.; Donini, O.; Cieplak, P.; Srinivasan, J.; Case, D. A.; Cheatham, T. E. Calculating Structures and Free Energies of Complex Molecules: Combining Molecular Mechanics and Continuum Models. *Acc. Chem. Res.* **2000**, *33*, 889–897.

(36) Homeyer, N.; Stoll, F.; Hillisch, A.; Gohlke, H. Binding Free Energy Calculations for Lead Optimization: Assessment of Their Accuracy in an Industrial Drug Design Context. *J. Chem. Theory Comput.* **2014**, *10*, 3331–3344.

(37) Zhang, X.; Wong, S. E.; Lightstone, F. C. Toward Fully Automated High Performance Computing Drug Discovery: A Massively Parallel Virtual Screening Pipeline for Docking and Molecular Mechanics/generalized Born Surface Area Rescoring to Improve Enrichment. *J. Chem. Inf. Model.* **2014**, *54*, 324–337.

(38) Li, Y.; Liu, Z.; Wang, R. Test MM-PB/SA on True Conformational Ensembles of Protein - Ligand Complexes. **2010**, 1682–1692.

(39) Huanga, D.; Caflischa, A. Library Screening by Fragment-Based Docking. *J. Mol. Recognit.* **2010**, *23*, 183–193.

(40) Sabbadin, D.; Ciancetta, A.; Moro, S. Bridging Molecular Docking to Membrane Molecular Dynamics to Investigate GPCR − Ligand Recognition: The Human A_2A Adenosine Receptor as a Key Study. *J. Chem. Inf. Model.* **2014**, *54*, 169–183.

(41) Tarcsay, A.; Paragi, G. G.; Vass, M.; Jojart, B.; Bogár, F.; Keseru, G. M.; Jójárt, B.; Keserű, G. M. The Impact of Molecular Dynamics Sampling on the Performance of Virtual Screening against GPCRs. *J. Chem. Inf. Model.* **2013**, *53*, 59–67.

(42) Ng, H. W.; Laughton, C. A.; Doughty, S. W. Molecular Dynamics Simulations of the Adenosine A2a Receptor in POPC and POPE lipid bilayers: effects of membrane on protein behavior. *J. Chem. Inf. Model.* **2014**, *54*, 573-581.

(43) Ng, H. W.; Laughton, C. A.; Doughty, S. W. Molecular Dynamics Simulations of the Adenosine A2a Receptor: Structural Stability, Sampling, and Convergence. *J. Chem. Inf. Model.* **2013**, *53*, 1168–1178.

(44) Li, J.; Jonsson, A. L.; Beuming, T.; Shelley, J. C.; Voth, G. A. Ligand-Dependent Activation and Deactivation of the Human Adenosine A(2A) Receptor. *J. Am. Chem. Soc.* **2013**, *135*, 8749–8759.

(45) Sabbadin, D.; Ciancetta, A.; Deganutti, G.; Cuzzolin, A.; Moro, S. Exploring the Recognition Pathway at the Human A2A Adenosine Receptor of the Endogenous Agonist Adenosine Using Supervised Molecular Dynamics Simulations. *Med. Chem. Commun.* **2015**, *6*, 1081–1085.

(46) Lavecchia, A.; Di Giovanni, C. Virtual Screening Strategies in Drug Discovery: A Critical Review. *Curr. Med. Chem.* **2013**, *20*, 2839–2860.

(47) Desmond Molecular Dynamics System, Version 3.0, D.E. Shaw Research, New York, NY, 2011.

(48) *Maestro-Desmond Interoperability Tools*, version 3.1; Schrodinger: New York, NY, 2012.

(49) Jorgensen, W. L.; Maxwell, D. S.; Tirado-Rives, J. Development and Testing of the OLPS All-Atom Force Field on Conformational Energetics and Properties of Organic Liquids. *J. Am. Chem. Soc.* **1996**, *118*, 11225–11236.

(50) Kaminski, G. A.; Friesner, R. A.; Tirado-Rives, J.; Jorgensen, W. L. Comparison with Accurate

Quantum Chemical Calculations on Peptides. *J. Phys. Chem. B* **2001**, *105*, 6474–6487.

(51) Shivakumar, D.; Williams, J.; Wu, Y. J.; Damm, W.; Shelley, J.; Sherman, W. Prediction of Absolute Solvation Free Energies Using Molecular Dynamics Free Energy Perturbation and the OPLS Force Field. *J. Chem. Theory Comput.* **2010**, *6*, 1509–1519.

(52) Case, D. A.; Babin, V.; Berryman, J. T.; Betz, R. M.; Cai, Q.; Cerutti, D. S.; Cheatham, III, T. E.; Darden, T. A.; Duke,R. E.; Gohlke, H.; Goetz, A. W.; Gusarov, S.; Homeyer, N.; Janowski, P.; Kaus, J.; Kolossváry, I.; Kovalenko, A.; Lee, T. S.; LeGrand, S.; Luchko, T.; Luo, R.; Madej, B.; Merz, K. M.; Paesani, F.; Roe, D. R.; Roitberg, A.; Sagui, C.; Salomon-Ferrer, R.; Seabra, G.; Simmerling, C. L.; Smith, W.; Swails, J.; Walker, R. C.; Wang, J.; Wolf, R. M.; Wu, X.; Kollman, P. A. AMBER *14*; University of California: San Francisco, CA, 2014.

(53) Maier, J. A.; Martinez, C.; Kasavajhala, K.; Wickstrom, L.; Hauser, K. E.; Simmerling, C. ff14SB: Improving the Accuracy of Protein Side Chain and Backbone Parameters from ff99SB. *J. Chem. Theory Comput.* **2015**, *11*, 3696–3713.

(54) Hawkins, P. C. D.; Skillman, A. G.; Warren, G. L.; Ellingson, B. A.; Stahl, M. T. Conformer Generation with OMEGA: Algorithm and Validation Using High Quality Structures from the Protein Databank and Cambridge Structural Database. *J. Chem. Inf. Model.* **2010**, *50*, 572–584.

(55) Hawkins, P. C. D.; Nicholls, A. Conformer Generation with OMEGA: Learning from the Data Set and the Analysis of Failures. *J. Chem. Inf. Model.* **2012**, *52*, 2919–2936.

(56) Hino, T.; Arakawa, T.; Iwanari, H.; Yurugi-Kobayashi, T.; Ikeda-Suno, C.; Nakada-Nakura, Y.; Kusano-Arai, O.; Weyand, S.; Shimamura, T.; Nomura, N.; Cameron, A. D.; Kobayashi, T.; Hamakubo, T.; Iwata, S.; Murata, T. G-Protein-Coupled Receptor Inactivation by an Allosteric Inverse-Agonist Antibody. *Nature* **2012**, *482*, 237–240.

(57) Liu, W.; Chun, E.; Thompson, A. A.; Chubukov, P.; Xu, F.; Katritch, V.; Han, G. W.; Roth, C. B.; Heitman, L. H.; IJzerman, A. P.; Cherezov, V.; Stevens, R. C. Structural Basis for Allosteric Regulation of GPCRs by Sodium Ions. *Science* **2012**, *337*, 232–236.

(58) Maestro, Version 8.5, Schrodinger, Inc. New York, NY, 2008.

(59) GOLD Suite, Version 5.2; Cambridge Crystallographic Data Centre: Cambridge, U. K., 2015.

(60) Jones, G.; Willett, P.; Glen, R. C.; Leach, A. R.; Taylor, R. Development and Validation of a Genetic Algorithm for Flexible Docking. *J. Mol. Biol.* **1997**, *267*, 727–748.

(61) Verdonk, M. L.; Chessari, G.; Cole, J. C.; Hartshorn, M. J.; Murray, C. W.; Nissink, J. W. M.; Taylor, R. D.; Taylor, R. Modeling Water Molecules in Protein-Ligand Docking Using GOLD. *J. Med. Chem.* **2005**, *48*, 6504–6515.

(62) Eldridge, M. D.; Murray, C. W.; Auton, T. R.; Paolini, G. V; Mee, R. P. Empirical Scoring Functions: I. The Development of a Fast Empirical Scoring Function to Estimate the Binding Affinity of Ligands in Receptor Complexes. *J. Comput. Aided. Mol. Des.* **1997**, *11*, 425–445.

(63) Korb, O.; Stützle, T.; Exner, T. E. Empirical Scoring Functions for Advanced Protein-Ligand Docking with PLANTS. *J. Chem. Inf. Model.* **2009**, *49*, 84–96.

(64) Hawkins, P. C. D.; Skillman, A. G.; Nicholls, A. Comparison of Shape-Matching and Docking as Virtual Screening Tools. *J. Med. Chem.* **2007**, *50*, 74–82.

(65) Brooks, B. R.; Bruccoleri, R. E.; Olafson, B. D.; States, D. J.; Swaminathan, S.; Karplus, M. CHARMM: A Program for Macromolecular Energy, Minimization, and Dynamics Calculations. *J. Comput. Chem.* **1983**, *4*, 187–217.

(66) Brooks, B. R.; Brooks, C. L.; Mackerell, A. D.; Nilsson, L.; Petrella, R. J.; Roux, B.; Won, Y.; Archontis, G.; Bartels, C.; Boresch, S.; Caflisch, A.; Caves, L.; Cui, Q.; Dinner, A. R.; Feig, M.; Fischer, S.; Gao, J.; Hodoscek, M.; Im, W.; Kuczera, K.; Lazaridis, T.; Ma, J.; Ovchinnikov, V.; Paci, E.; Pastor, R. W.; Post, C. B.; Pu, J. Z.; Schaefer, M.; Tidor, B.; Venable, R. M.; Woodcock, H. L.; Wu, X.; Yang, W.; York, D. M.; Karplus, M. CHARMM: The Biomolecular Simulation Program. *J. Comput. Chem.* **2009**, *30*, 1545–1614.

(67) Kolb, P.; Caflisch, A. Automatic and Efficient Decomposition of Two-Dimensional Structures

of Small Molecules for Fragment-Based High-Throughput Docking. *J. Med. Chem.* **2006**, *49*, 7384–7392.

(68) Warwicker, J.; Watson, H. C. Calculation of the Electric Potential in the Active due to a-Helix Dipoles Site Cleft. *J. Mol. Biol.* **1982**, *157*, 671–679.

(69) Im, W.; Beglov, D.; Roux, B. Continuum Solvation Model: Computation of Electrostatic Forces from Numerical Solutions to the Poisson-Boltzmann Equation. *Comput. Phys. Commun.* **1998**, *111*, 59–75.

(70) Katritch, V.; Kufareva, I.; Abagyan, R. Structure Based Prediction of Subtype-Selectivity for Adenosine Receptor Antagonists. *Neuropharmacology* **2011**, *60*, 108–115.

(71) Floris, M.; Sabbadin, D.; Medda, R.; Bulfone, A.; Moro, S. Adenosiland: Walking through Adenosine Receptors Landscape. *Eur. J. Med. Chem.* **2012**, *58*, 248–257.

(72) Sali, A.; Blundell, T. L. Comparative Protein Modelling by Satisfaction of Spatial Restraints. *J. Mol. Biol.* **1993**, *234*, 779–815.

(73) Fiser, A.; Do, R. K.; Sali, A. Modeling of Loops in Protein Structures. *Protein Sci.* **2000**, *9*, 1753–1773.

(74) Massotte, D.; Kieffer, B. L. The Second Extracellular Loop: A Damper for G Protein-Coupled Receptors? *Nat. Struct. Mol. Biol.* **2005**, *12*, 287–288.

(75) Nguyen, A. T.; Vecchio, E. A.; Thomas, T.; Nguyen, T. D.; Aurelio, L.; Scammels, P. J.; White, P. J.; Sexton, P. M.; Gregory, K. J.; May, L. T.; Christopoulos, A. The Role of the Second Extracellular Loop of the Adenosine A1 Receptor on Allosteric Modulator Binding, Signaling and Cooperativity. *Mol. Pharmacol.* **2016**, *90*, 715–725.

(76) Schiedel, A. C.; Hinz, S.; Thimm, D.; Sherbiny, F.; Borrmann, T.; Maaß, A.; Müller, C. E. The Four Cysteine Residues in the Second Extracellular Loop of the Human Adenosine A 2B Receptor: Role in Ligand Binding and Receptor Function. *Biochem. Pharmacol.* **2011**, *82*, 389–399.

(77) De Filippo, E.; Namasivayam, V.; Zappe, L.; El-Tayeb, A.; Schiedel, A. C.; Müller, C. E. Role of Extracellular Cysteine Residues in the Adenosine A2A Receptor. *Purinergic Signal.* **2016**, *12*, 313–329.

(78) Halgren, T. A. Merck Molecular Force Field. I. Basis, Form, Scope, Parameterization, and Performance of MMFF94. *J. Comput. Chem.* **1996**, *17*, 490–519.

(79) Halgren, T. A. MMFF VII. Characterization of MMFF94, MMFF94s, and Other Widely Available Force Fields for Conformational Energies and for Intermolecular-Interaction Energies and Geometries. *J. Comput. Chem.* **1999**, *20*, 730–748.

(80) Pettersen, E. F.; Goddard, T. D.; Huang, C. C.; Couch, G. S.; Greenblatt, D. M.; Meng, E. C.; Ferrin, T. E. UCSF Chimera - A Visualization System for Exploratory Research and Analysis. *J. Comput. Chem.* **2004**, *25*, 1605–1612.

(81) Mori, T.; Ogushi, F.; Sugita, Y. Analysis of Lipid Surface Area in Protein-Membrane Systems Combining Voronoi Tessellation and Monte Carlo Integration Methods. *J. Comput. Chem.* **2012**, *33*, 286–293.

(82) Dickson, C. J.; Madej, B. D.; Skjevik, Å. A.; Betz, R. M.; Teigen, K.; Gould, I. R.; Walker, R. C. Lipid14: The Amber Lipid Force Field. *J. Chem. Theory Comput.* **2014**, *10*, 865–879.

(83) Lomize, M. A.; Lomize, A. L.; Pogozheva, I. D.; Mosberg, H. I. OPM: Orientations of Proteins in Membranes Database. *Bioinformatics* **2006**, *22*, 623–625.

(84) Jorgensen, W. L.; Chandrasekhar, J.; Madura, J. D.; Impey, R. W.; Klein, M. L. Comparison of Simple Potential Functions for Simulating Liquid Water. *J. Chem. Phys.* **1983**, *79*, 926–936.

(85) Darden, T.; York, D.; Pedersen, L. Particle Mesh Ewald: An N·log(N) Method for Ewald Sums in Large Systems. *J. Chem. Phys.* **1993**, *98*, 10089–10092.

(86) Essmann, U.; Perera, L.; Berkowitz, M. L.; Darden, T.; Lee, H.; Pedersen, L. G. A Smooth Particle Mesh Ewald Method. *J. Chem. Phys.* **1995**, *103*, 8577–8593.

(87) Martyna, G. J.; Tobias, D. J.; Klein, M. L. Constant Pressure Molecular Dynamics Algorithms. *J. Chem. Phys.* **1994**, *101*, 4177–4189.

(88) Humphreys, D. D.; Friesner, R. A.; Berne, B. J. A Multiple-Time-Step Molecular Dynamics Algorithm for Macromolecules. *J. Phys. Chem.* **1994**, *98*, 6885–6892.

(89) Koynova, R.; Caffrey, M. Phases and Phase Transitions of the Phosphatidylcholines. *Biochim. Biophys. Acta - Rev. Biomembr.*, **1998**, *1376*, 91–145.

(90) Dupradeau, F.-Y.; Pigache, A.; Zaffran, T.; Savineau, C.; Lelong, R.; Grivel, N.; Lelong, D.; Rosanski, W.; Cieplak, P. The R.E.D. Tools: Advances in RESP and ESP Charge Derivation and Force Field Library Building. *Phys. Chem. Chem. Phys.* **2010**, *12*, 7821–7839.

(91) Zgarbova, M.; Otyepka, M.; Sponer, J.; Mladek, A.; Banas, P.; Cheatham III, T. E. C.; Jurecka, P. Refinement of the Cornell et Al. Nucleic Acid Force Field Based on Reference Quantum Chemical Calculations of Torsion Profiles of the Glycosidic Torsion. *J. Chem. Theory Comput.* **2011**, *7*, 2886– 2802.

(92) Sastry, M.; Lowrie, J. F.; Dixon, S. L.; Sherman, W. Large-Scale Systematic Analysis of 2D Fingerprint Methods and Parameters to Improve Virtual Screening Enrichments. *J. Chem. Inf. Model.* **2010**, *50*, 771–784.

(93) Gaulton, A.; Bellis, L. J.; Bento, A. P.; Chambers, J.; Davies, M.; Hersey, A.; Light, Y.; McGlinchey, S.; Michalovich, D.; Al-Lazikani, B.; Overington, J. P. ChEMBL: A Large-Scale Bioactivity Database for Drug Discovery. *Nucleic Acids Res.* **2012**, *40*, D1100-1107.

(94) Bento, A. P.; Gaulton, A.; Hersey, A.; Bellis, L. J.; Chambers, J.; Davies, M.; Krüger, F. A.; Light, Y.; Mak, L.; McGlinchey, S.; Nowotka, M.; Papadatos, G.; Santos, R.; Overington, J. P. The ChEMBL Bioactivity Database: An Update. *Nucleic Acids Res.* **2014**, *42*, D1083-1090.

(95) Klotz, K.-N.; Hessling, J.; Hegler, J.; Owman, C.; Kull, B.; Fredholm, B. B.; Lohse, M. J. Comparative Pharmacology of Human Adenosine Receptor Subtypes – Characterization of Stably Transfected Receptors in CHO Cells. *Naunyn. Schmiedebergs. Arch. Pharmacol.* **1997**, *357*, 1–9.

(96) Kent, R. S.; De Lean, A.; Lefkowitz, R. J. A Quantitative Analysis of Beta-Adrenergic Receptor Interactions: Resolution of High and Low Affinity States of the Receptor by Computer Modeling of Ligand Binding Data. *Mol. Pharmacol.* **1980**, *17*, 14–23.

(97) Klotz, K. N.; Cristalli, G.; Grifantini, M. Photoaffinity Labeling of A1-Adenosine Receptors. *J. Biol. Chem.* **1985**, *260*, 14659–14664.

(98) Tuccinardi, T.; Nuti, E.; Ortore, G.; Rossello, A.; Avramova, S. I.; Martinelli, A. Development of a Receptor-Based 3D-QSAR Study for the Analysis of MMP2, MMP3, and MMP9 Inhibitors. *Bioorg. Med. Chem.* **2008**, *16*, 7749–7758.

(99) Shoichet, B. K. Screening in a Spirit Haunted World. *Drug Discovery Today* **2006**, *11*, 607–615.

(100) Bruns, R. F.; Fergus, J. H. Allosteric Enhancement of Adenosine A1 Receptor Binding and Function by 2-Amino-3-Benzoylthiophenes. *Mol. Pharmacol.* **1990**, *38*, 939–949.

(101) Kourounakis, A.; Visser, C.; De Groote, M.; IJzerman, A. P. Differential Effects of the Allosteric Enhancer (2-Amino-4,5-Dimethyl-trienyl)[3-(Trifluoromethyl) Phenyl]methanone (PD81,723) on Agonist and Antagonist Binding and Function at the Human Wild-Type and a Mutant (T277A) Adenosine A1 Receptor. *Biochem. Pharmacol.* **2001**, *61*, 137–144.

(102) Nikolakopoulos, G.; Figler, H.; Linden, J.; Scammells, P. J. 2-Aminothiophene-3-Carboxylates and Carboxamides as Adenosine A1 Receptor Allosteric Enhancers. *Bioorg. Med. Chem.* **2006**, *14*, 2358–2365.

(103) Romagnoli, R.; Baraldi, P. G.; Moorman, A. R.; Borea, P. A.; Varani, K. Current Status of A1 Adenosine Receptor Allosteric Enhancers. *Future Med. Chem.* **2015**, *7*, 1247–1259.

(104) Valant, C.; Aurelio, L.; Devine, S. M.; Ashton, T. D.; White, J. M.; Sexton, P. M.; Christopoulos, A.; Scammells, P. J. Synthesis and Characterization of Novel 2-Amino-3-

Benzoylthiophene Derivatives as Biased Allosteric Agonists and Modulators of the Adenosine A1 Receptor. *J. Med. Chem.* **2012**, *55*, 2367–2375.

(105) Tranberg, C. E.; Zickgraf, A.; Giunta, B. N.; Luetjens, H.; Figler, H.; Murphree, L. J.; Falke, R.; Fleischer, H.; Linden, J.; Scammells, P. J.; Olsson, R. A. 2-Amino-3-Aroyl-4,5-Alkylthiophenes: Agonist Allosteric Enhancers at Human a1 Adenosine Receptors. *J. Med. Chem.* **2002**, *45*, 382–389.

(106) Ferguson, G. N.; Valant, C.; Horne, J.; Figler, H.; Flynn, B. L.; Linden, J.; Chalmers, D. K.; Sexton, P. M.; Christopoulos, A.; Scammells, P. J. 2-Aminothienopyridazines as Novel Adenosine A1 Receptor Allosteric Modulators and Antagonists. *J. Med. Chem.* **2008**, *51*, 6165–6172.

(107) Baell, J. B.; Holloway, G. A. New Substructure Filters for Removal of Pan Assay Interference Compounds (PAINS) from Screening Libraries and for Their Exclusion in Bioassays. *J. Med. Chem.* **2010**, *53*, 2719–2740.

(108) Capuzzi, S. J.; Muratov, E. N.; Tropsha, A. Phantom PAINS: Problems with the Utility of Alerts for Pan-Assay Interference Compounds. *J. Chem. Inf. Model.* **2017**, *57*, 417–427.

(109) Jasial, S.; Hu, Y.; Bajorath, J. How Frequently Are Pan Assay Interference Compounds Active? Large-Scale Analysis of Screening Data Reveals Diverse Activity Profiles, Low Global Hit Frequency, and Many Consistently Inactive Compounds. *J. Med. Chem.* **2017**, 60, 3879−3886.

(110) Kiss, L. E.; Ferreira, H. S.; Torrão, L.; Bonifácio, M. J.; Palma, P. N.; Soares-da-Silva, P.; Learmonth, D. A. Discovery of a Long-Acting, Peripherally Selective Inhibitor of Catechol-O-Methyltransferase. *J. Med. Chem.* **2010**, *53*, 3396–3411.

(111) http://www.cbligand.org/PAINS/. PAINS.

(112) Homeyer, N.; Ioannidis, H.; Kolarov, F.; Gauglitz, G.; Zikos, C.; Kolocouris, A.; Gohlke, H. Interpreting Thermodynamic Profiles of Aminoadamantane Compounds Inhibiting the M2 Proton Channel of Influenza A by Free Energy Calculations. *J. Chem. Inf. Model.* **2016**, *56*, 110–126.

(113) Homeyer, N.; Gohlke, H. FEW: A Workflow Tool for Free Energy Calculations of Ligand Binding. *J. Comput. Chem.* **2013**, *34*, 965–973.

(114) Matricon, P.; Ranganathan, A.; Warnick, E.; Gao, Z.-G.; Rudling, A.; Lambertucci, C.; Marucci, G.; Ezzati, A.; Jaiteh, M.; Dal Ben, D.; Jacobson, K. A.; Carlsson, J. Fragment Optimization for GPCRs by Molecular Dynamics Free Energy Calculations: Probing Druggable Subpockets of the A2A Adenosine Receptor Binding Site. *Sci. Rep.* **2017**, *7*, 6398–6409.

(115) Gkeka, P.; Eleftheratos, S.; Kolocouris, A.; Cournia, Z. Free Energy Calculations Reveal the Origin of Binding Preference for Aminoadamantane Blockers of Influenza A/M2TM Pore. *J. Chem. Theory Comput.* **2013**, *9*, 1272–1281.

(116) Ioannidis, H.; Drakopoulos, A.; Tzitzoglaki, C.; Homeyer, N.; Kolarov, F.; Gkeka, P.; Freudenberger, K.; Liolios, C.; Gauglitz, G.; Cournia, Z.; Gohlke, H.; Kolocouris, A. Alchemical Free Energy Calculations and Isothermal Titration Calorimetry Measurements of Aminoadamantanes Bound to the Closed State of Influenza A/M2TM. *J. Chem. Inf. Model.* **2016**, *56*, 862–876.

(117) Dal Ben, D.; Lambertucci, C.; Marucci, G.; Volpini, R.; Cristalli, G. Adenosine Receptor Modeling: What Does the A2A Crystal Structure Tell Us? *Curr. Top. Med. Chem.* **2010**, *10*, 993–1018.

(118) Ivanov, A.; Barak, D.; Jacobson, K. Evaluation of Homology Modeling of G Protein-Coupled Receptors in Light of the A2A Adenosine Receptor Crystallographic Structure. *J. Med. Chem.* **2009**, *52*, 3284–3292.

(119) Leal, C. M.; Pereira, S. L.; Kümmerle, A. E.; Leal, D. M.; Tesch, R.; De Sant'Anna, C. M. R.; Fraga, C. A. M.; Barreiro, E. J.; Sudo, R. T.; Zapata-Sudo, G. Antihypertensive Profile of 2-Thienyl-3,4-Methylenedioxybenzoylhydrazone Is Mediated by Activation of the A2A

Adenosine Receptor. *Eur. J. Med. Chem.* **2012**, *55*, 49–57.

(120) Thimm, D.; Schiedel, A. C.; Sherbiny, F. F.; Hinz, S.; Hochheiser, K.; Bertarelli, D. C.; Maaß, A.; Müller, C. E. Ligand-specific binding and activation of the human adenosine A2B receptor. *Biochemistry* **2013**, *52*, 726–740.

(121) Wu, J.-P.; Fleck, R.; Brickwood, J.; Capolino, A.; Catron, K.; Chen, Z.; Cywin, C.; Emeigh, J.; Foerst, M.; Ginn, J.; Hrapchak, M.; Hickey, E.; Hao, M.-H.; Kashem, M.; Li, J.; Liu, W.; Morwick, T.; Nelson, R.; Marshall, D.; Martin, L.; Nemoto, P.; Potocki, I.; Liuzzi, M.; Peet, G. W.; Scouten, E.; Stefany, D.; Turner, M.; Weldon, S.; Zimmitti, C.; Spero, D.; Kelly, T. a. The Discovery of Thienopyridine Analogues as Potent IkappaB Kinase Beta Inhibitors. Part II. *Bioorg. Med. Chem. Lett.* **2009**, *19*, 5547–5551.

(122) Liu, W.; Chun, E.; Thompson, A. A; Chubukov, P.; Xu, F.; Katritch, V.; Han, G. W.; Roth, C. B.; Heitman, L. H.; IJzerman, A. P.; Cherezov, V.; Stevens, R. C. Structural Basis for Allosteric Regulation of GPCRs by Sodium Ions. *Science* **2012**, *337*, 232–236.

(123) Lebon, G.; Warne, T.; Edwards, P. C.; Bennett, K.; Langmead, C. J.; Leslie, A. G. W.; Tate, C. G. Agonist-Bound Adenosine A2A Receptor Structures Reveal Common Features of GPCR Activation. *Nature* **2011**, *474*, 521–525.

(124) Jazayeri, A.; Dias, J. M.; Marshall, F. H. From G Protein-Coupled Receptor Structure Resolution to Rational Drug Design. *J. Biol. Chem.* **2015**, *290*, 19489–19495.

11 Schemes and Figures captions

Scheme 1. Workflow used for the discovery of new hits.

Figure 1. Predicted binding mode for ligand **13 i**n the orthosteric site of the A$_{2A}$AR. (a) Top-view of the orthosteric binding site. Sidechains of amino acids important for binding are shown in blue sticks. (b) Lateral view of the complex, facing helices TM6 and TM7, with the structure of TM7 partially omitted. MD optimization of the docking pose showed that **13** can adopt a binding orientation in which the amino group of the thiophene ring is hydrogen-bonded to the carbonyl of amide group of N(6.55) and the carboxylate of E(5.30) in EL2. The thiophene ring has an aromatic π-π stacking interaction with the conserved F(5.29) (EL2) and forms important hydrophobic contacts with I(7.39), while the sulfur atom forms H-bonds with the amide group of N(6.55). In panel (a) side chains of amino acids important for binding are displayed in blue sticks. In panel (b) side chains of amino acids important for binding are displayed as gray sticks. Binding orientation of the ligand after the MD simulation is shown in yellow sticks and sidechains of some amino acids involved in ligand binding are displayed as gray sticks while the starting ligand and N(6.55)/E(5.30) side chain positions are shown in green wires. Hydrogen atoms are omitted except for those involved in hydrogen bond interactions, highlighted as black dashed lines. MD simulations of **13** in complex with the ARs were performed for 100 ns.

Figure 2. Top view and side view of the predicted binding mode for ligand **13** in the orthosteric site of the A$_1$AR. In panel (a) the sidechains of amino acids important for binding are displayed in yellow sticks. In panel (b) the sidechains of amino acids important for binding are displayed as gray sticks. Binding orientation of the ligand after the MD simulation is shown in yellow sticks and sidechains of some amino acids involved in ligand binding are displayed as gray sticks while the starting ligand and N(6.55)/E(5.30) side chain positions are shown in green wires. Hydrogen atoms are omitted except for those involved in hydrogen bond interactions, highlighted as black dashed lines. MD simulations of **13** in complex with the ARs were performed for 100 ns.

Figure 3. Top view and side of the predicted binding mode for ligand **13** in the orthosteric site of the A$_3$AR. In panel (a) the sidechains of amino acids important for binding are displayed in pink sticks. In panel (b) the sidechains of amino acids important for binding are displayed as gray sticks. Binding orientation of the ligand after the MD simulation is shown in yellow sticks and sidechains of some

amino acids involved in ligand binding are displayed as gray sticks while the starting ligand and N(6.55)/E(5.30) side chain positions are shown in green wires. Hydrogen atoms are omitted except for those involved in hydrogen bond interactions, highlighted as black dashed lines. MD simulations of **13** in complex with the ARs were performed for 100 ns.

Figure 4. The MD simulations of the docking pose of **11** against A_{2A} (panel a), A_1AR (panel b) showed that the binding orientation is not stable, probably due to the steric crowding induced by the cyclohexyl ring. (c) In contrast, MD simulations for 100 ns showed that the binding region of A_3AR can accommodate the cyclohexyl ring and ligand **11** can adopt a binding orientation in which the amino group and sulfur atom of the thiophene ring can form H-bonding interactions with N(6.55). The sidechains of some amino acids involved in ligand binding are displayed as gray sticks. Binding orientation of the ligand after the MD simulation is shown in yellow sticks and sidechains of some amino acids involved in ligand binding are displayed as gray sticks while the starting ligand and N(6.55)/E(5.30) side chain positions are shown in green wires. Hydrogen atoms are omitted except for those involved in hydrogen bond interactions, highlighted as black dashed lines.

Figure 5. (a) MD simulations of the docking pose of **1** against A_1AR showed that the binding orientation is not stable, probably because binding site is narrower for A_1AR. (b) In contrast MD simulations for 100 ns showed that the binding region of $A_{2A}AR$, and (c) of A_3AR can accommodate the ligand which adopts a binding orientation where the amino group and thiophene sulfur atom can form H-bond interactions with N(6.55). Sidechains of the amino acids crucial for ligand binding are displayed as gray sticks. Binding orientation of the ligand after the MD simulation is shown in yellow sticks and sidechains of some amino acids involved in ligand binding are displayed as gray sticks while the starting ligand and N(6.55)/E(5.30) side chain positions are shown in green wires. Hydrogen atoms are omitted except for those involved in hydrogen bond interactions, highlighted as black dashed lines.

Figure 6. Predicted binding modes before and after 100 ns MD simulations for ligand **17** **i**n the orthosteric binding site of (a) A_1, (b) A_{2A} and (c) A_3AR, resulting in stable complexes. Compound **17** can adopt a binding orientation inside $A_{2A}AR$ in which the amido group of thiophene ring is hydrogen-bonded to N(6.55) and E(5.30), and van der Waals interactions stabilize the ligand inside the binding cavity. The replacement of E(5.30) with V in A_3AR orthosteric cavity (panel c) retained the binding of compound **17**, as a result of hydrogen-bonding to N(6.55) and additional favourable van der Waals

interactions of its bulky lipophilic group in the vicinity of V(5.30). In A_1AR, which has a broader binding cavity, the 5-aryl-thiophene ring is inclined and the 3-NHCOR substituent is directed towards TM2. Binding orientation of the ligand after the MD simulation is shown in yellow sticks and sidechains of some amino acids involved in ligand binding are displayed as gray sticks while the starting ligand and N(6.55)/E(5.30) side chain positions are shown in green wires. Hydrogen atoms are omitted except for those involved in hydrogen bond interactions, highlighted as black dashed lines.

Figure 7. (a) Predicted binding of ligand **5** in the orthosteric binding area of the $A_{2A}AR$ using docking calculations and MD simulations, with the docking pose being used as a starting structure. The ligand was stabilized inside the $A_{2A}AR$ binding area between TM5, TM6 and TM2, with its monoaryl group close to TM5 and the phenyl-isoxazolyl substituent close to TM2. (b) This area is wider and the ligand cannot bind tightly inside A_1AR. (c) Binding of **5** inside A_3AR is highly favoured and the ligand engaged in many stabilizing interactions. In the depicted binding orientation the phenyl group of the 3-phenyl-isoxazole interacts through attractive van der Waals forces with the iPr side chain of V(5.30) and the isoxazole forms an aromatic π-π stacking interaction with the phenyl group of F(5.29). The amino group of the carbonyloxycarboximidamide fragment is H-bonded to the amide side chain of N(6.55). Nitrogen and oxygen atoms of the isoxazole ring can be hydrogen-bonded to the NH groups of F(5.29) or V(5.30). The thiazolyl group can be hydrogen-bonded to N(6.55). Binding orientation of the ligand after the MD simulation is shown in yellow sticks and sidechains of some amino acids involved in ligand binding are displayed as gray sticks while the starting ligand and N(6.55)/E(5.30) side chain positions are shown in green wires. Hydrogen atoms are omitted except for those involved in hydrogen bond interactions, highlighted as black dashed lines.

Figure 8. Competition binding curves for selected compounds at the A_3 adenosine receptor. The curves show the result of single representative experiments for compounds **1** (class A), **17** (class B), and **25** (class D). The competing radioligand was [^{3}H]HEMADO (1 nM). The K_i values from these individual experiments were 3.4 μM (compound **1**), 0.96 μM (compound **17**), and 0.76 μM (compound **25**). The data were fitted assuming a one-site competition model.

12 Schemes and Figures

14400 compounds (Maybridge/HitFinder)

1. OMEGA (Random conformer generation) | **2.** Docking A_{2A} (ChemPLP) / Clustering

48230 docking poses

ROCS filtering on ZM241385 coordinates (PDB ID 3EML)

6000 docking poses

Re-scoring with CHARMM and PBEQ to account for desolvation

60 topscore compounds

Selection based on structural features and synthetic feasibility

8 compounds

Biological testing

5 active against A_{2A}/A_3 or A_3 (63% success)

Selection of another **19** compounds based on the 3 most synthetically feasible for further development (18/19 active)

27 (**8+19**) derived compounds

1. Docking to A_1, A_{2A}, A_{2B}, A_3

2. Inspection of the stability of the binding orientations by means of MD simulations (10 ns) in equilibrated POPE bilayers using Desmond/OPLS (RMSD ligand criterion)

3. Verification of the stability of binding orientations applying a) Longer MD simulations (100 ns) b) Amber/ff14sb

Scheme 1

Figure 1

Figure 2
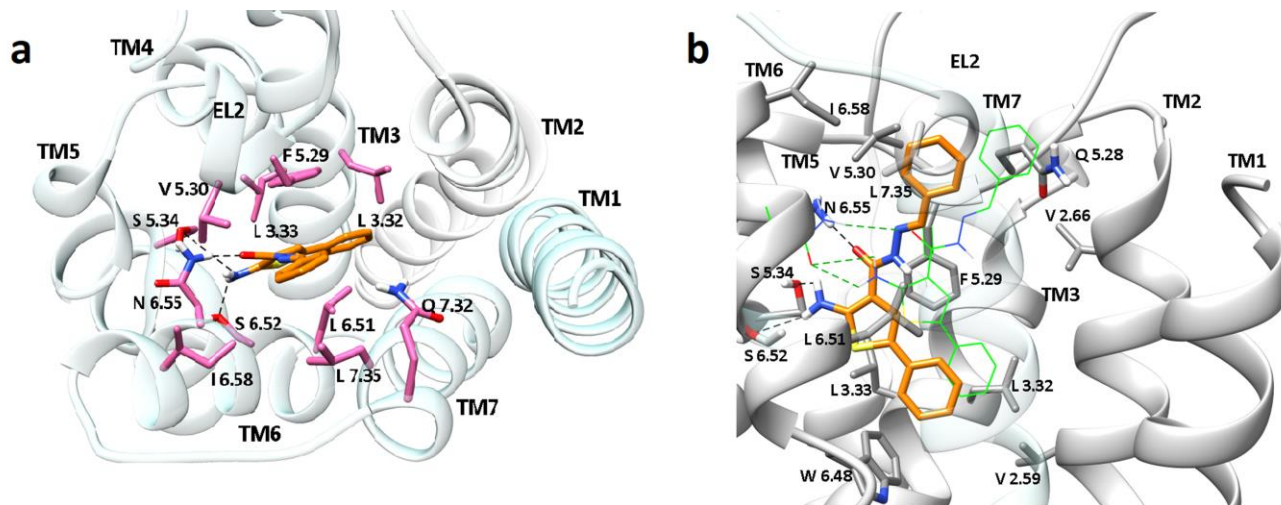
Figure 3
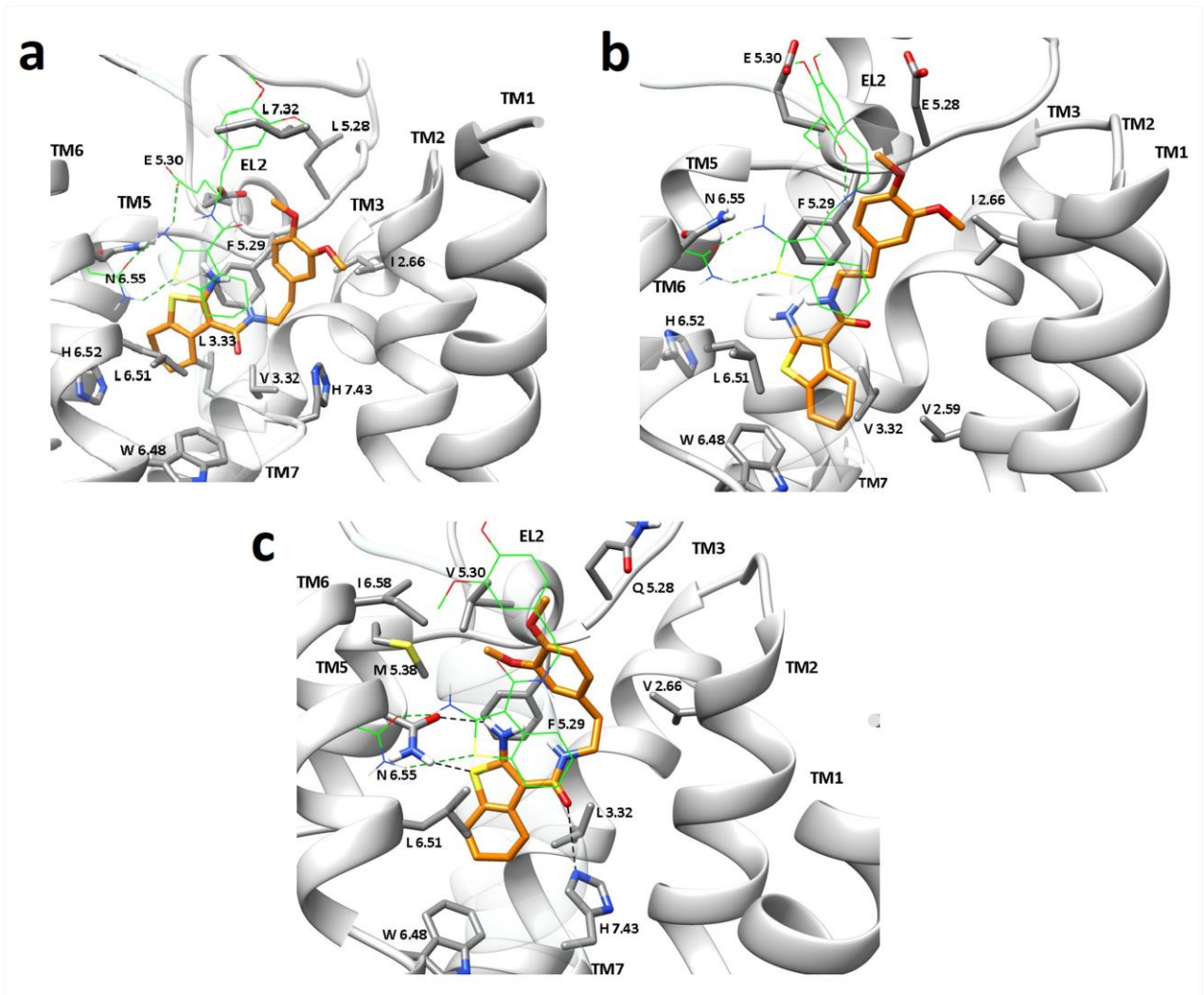
Figure 4
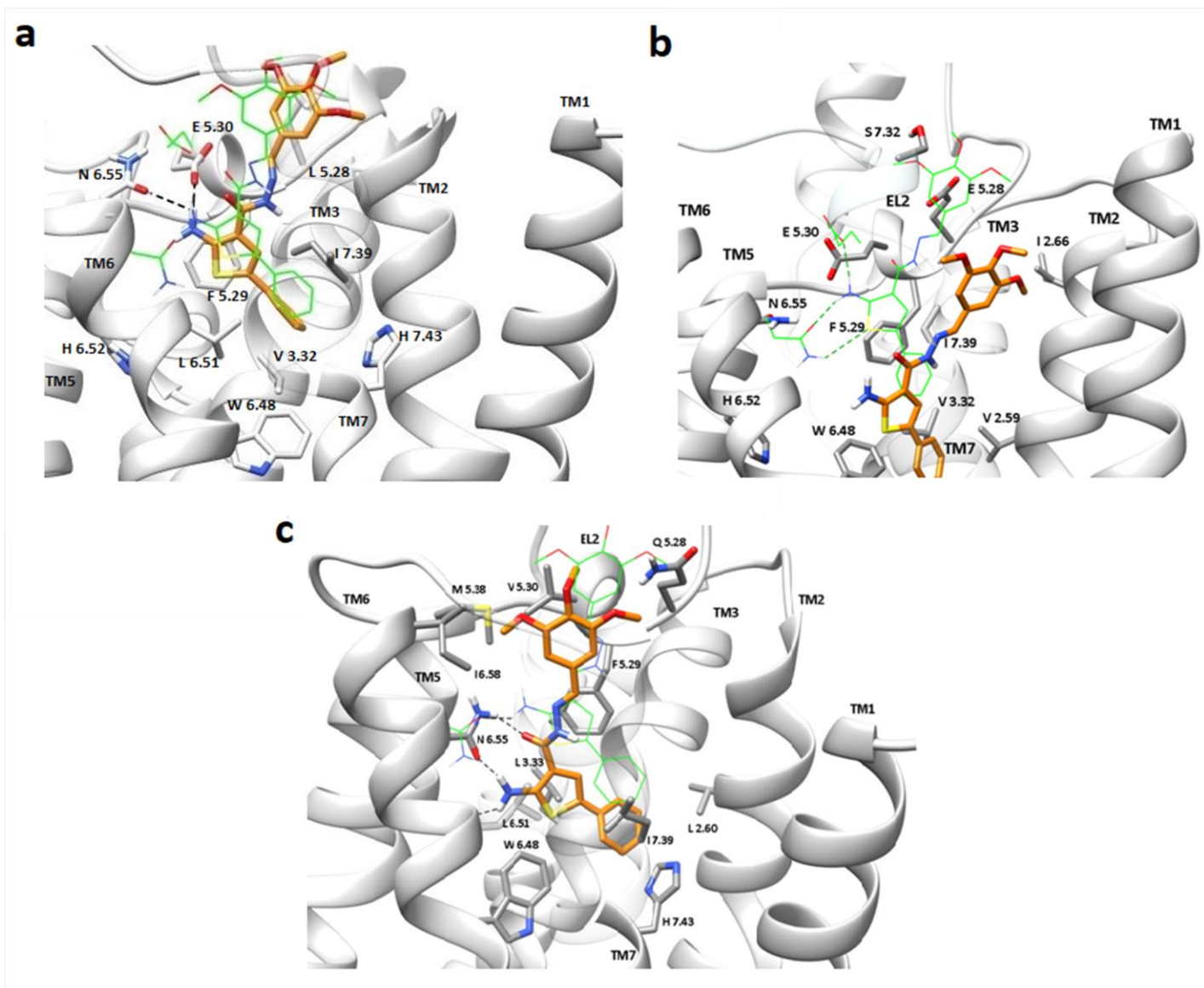
Figure 5
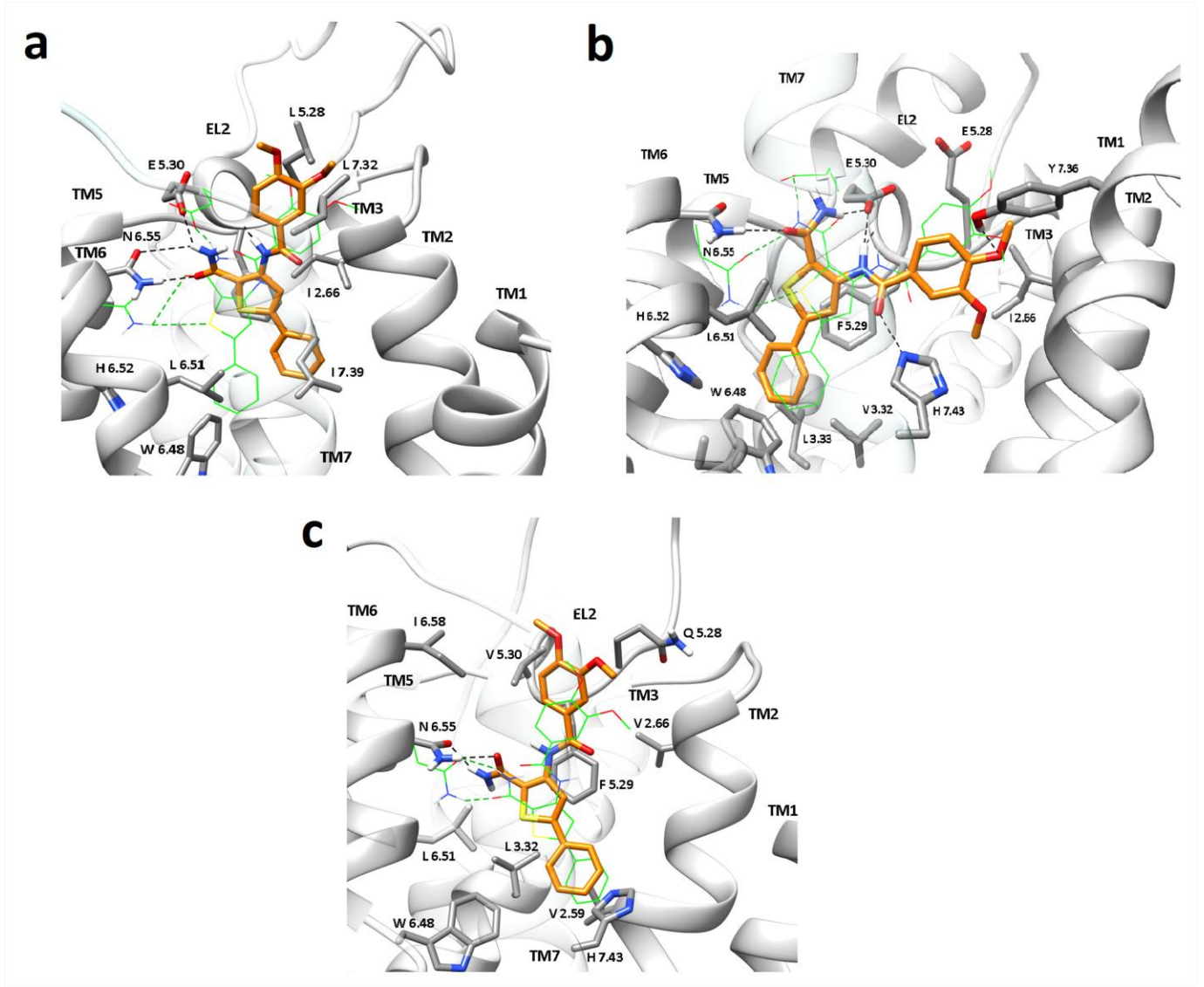
Figure 6
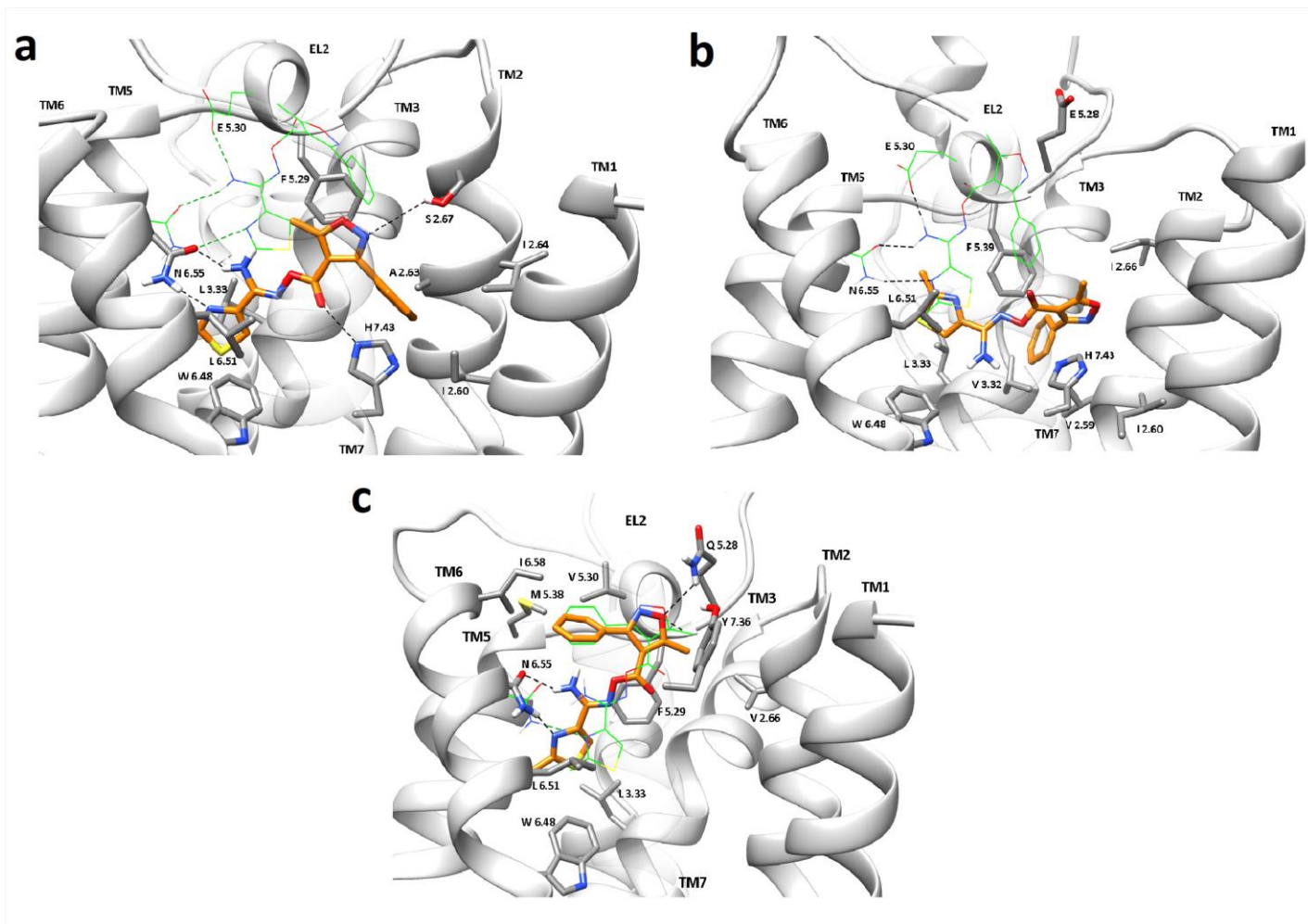
Figure 7
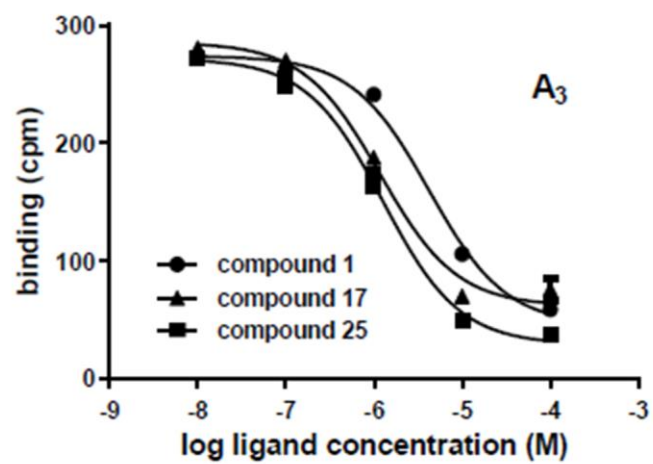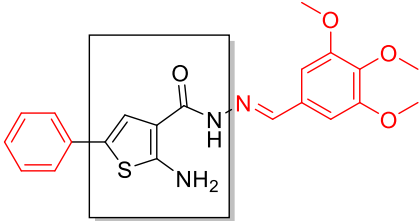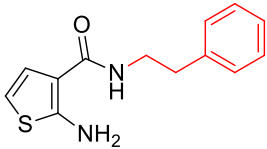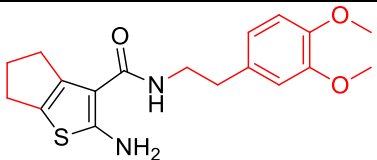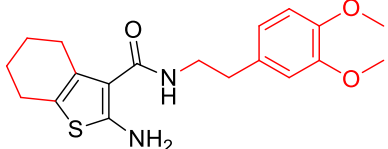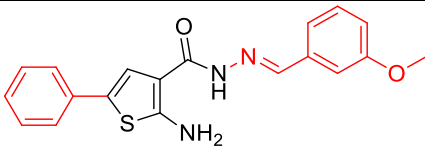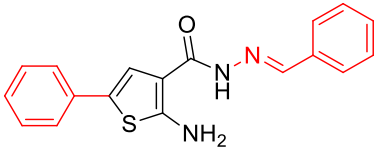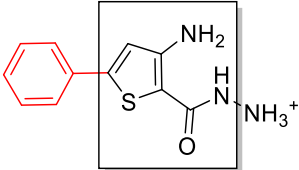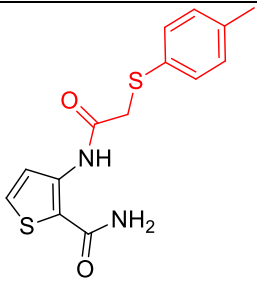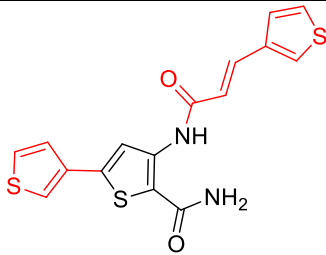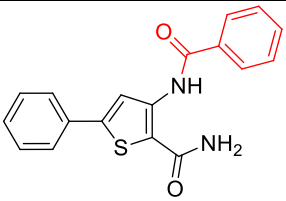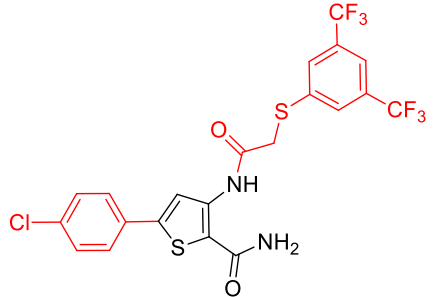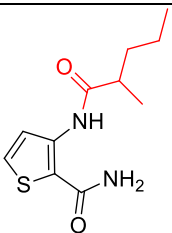
Figure 8
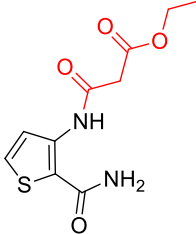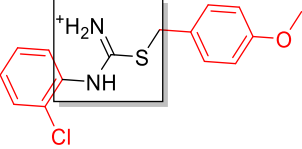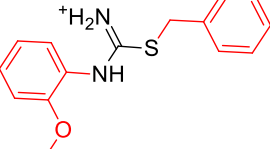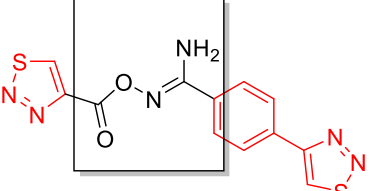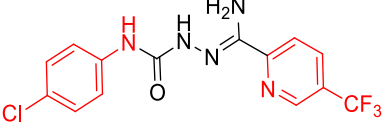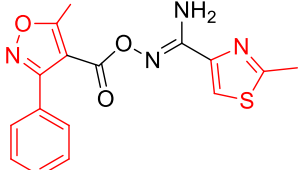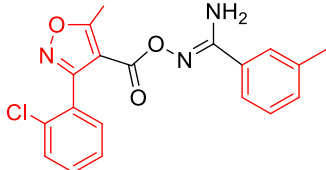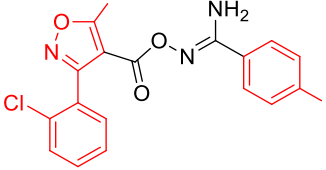
13 Tables
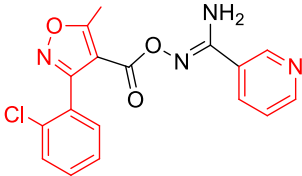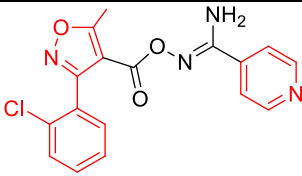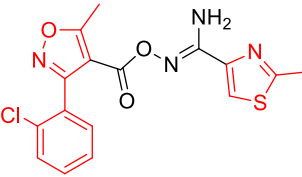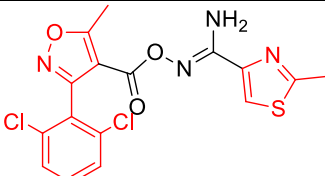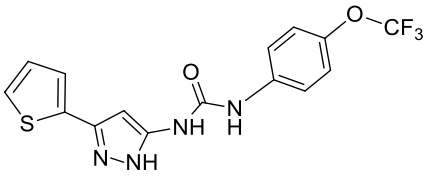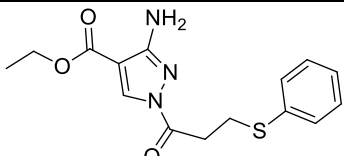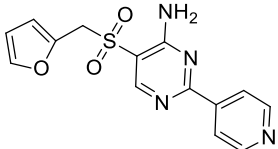
Table 1. Binding affinities obtained from radioligand binding assays and chemical structures of the eight hits (compounds **1-8**) from the docking screen and the 19 compounds (**9-27**) selected and tested based on the structures of **1**, **2** and **5** against the A_1, A_{2A}, A_{2B} [a] and A_3ARs.

Class	Compound number	Chemical structure	K_i (μM) [b]			T_c [c]
			A_1AR	$A_{2A}AR$	A_3AR	
A	1		>100	**2.67** (2.26-3.15)[e]	**3.10** (2.48-3.88)	0.22
A	9		>100	>60	**37.1** (23.0-60.0)[d]	0.32
A	10		>30	>60	**16.5** (11.2-24.3)	0.34
A	11		>30	>60	**14.8** (12.3-17.8)	0.34
A	12		>100	**3.93** (2.85-5.42)	**5.77** (5.34-6.23)	0.21
A	13		**15.2** (10.5-22)	**4.59** (3.18-6.63)	**5.16** (4.77-5.57)	0.24

		Structure				
B	14		>30	**31.7** (24.9-40.3)	**19.7** (11.6-33.4)	0.25
B	15		**7.48** (5.72-9.78)	>100	**5.39** (4.72-6.15)	0.16
B	16		**1.18** (1.09-1.28)	**4.69** (3.98-5.52)	**1.65** (1.24-2.21)	0.14
B	17		**1.09** (1.0-1.17)	**7.29** (6.86-7.76)	**0.918** (0.813-1.04)	0.19
B	18		>100	>100	**1.55** (1.25-1.93)	0.17
B	26		**7.33** (6.80-7.70)	>100	**27.4** (20.1-32.5)	0.20

|						
B	27		**18.0** (13.0-21.2)	>100	>100	0.18
C	2		≥100	**61.3** (52.6-71.5)	**16.6** (11.5-23.9)	0.17
C	19		>100	>100	>100	0.20
D	3		>100	>100	>100	0.13
D	4		≥100	>100	>100	0.14
D	5		>100	**21.8** (18.1-26.2)	**9.45** (8.75-10.2)	0.16
D	20		>100	>100	**30.9** (20.8-45.8)	0.16
D	21		**6.91** (6.36-7.52)	>100	**4.13** (3.38-5.04)	0.15

D	22		>60	>60	**4.49** (4.13-4.88)	0.16
D	23		>60	**30** (26.7-33.8)	**5.15** (4.51-5.88)	0.17
D	24		>30	>60	**4.16** (3.56-4.87)	0.16
D	25		>100	>100	**0.899** (0.766-1.060)	0.14
E	6		>100	>100	**30.6** (17-55)	0.21
E	7		>100	>100	**18.3** (10.3-32.7)	0.21
E	8		>100	≥100	>100	0.15

[a] All compounds did not exhibit binding evidence to $A_{2B}AR$. [b] Measured in three independent experiments. [c] Tanimoto similarity coefficient to the closest annotated AR ligand from ChEMBL (see Table S4).

TOC Graphic

Discovery of Novel Adenosine Receptor Antagonists through a Combined Structure- and Ligand-Based Approach Followed by Molecular Dynamics Investigation of Ligand Binding Mode

Panagiotis Lagarias, Eleni Vrontaki, George Lambrinidis, Dimitrios Stamatis, Marino Convertino, Gabriella Ortore, Thomas Mavromoustakos, Karl-Norbert Klotz, Antonios Kolocouris
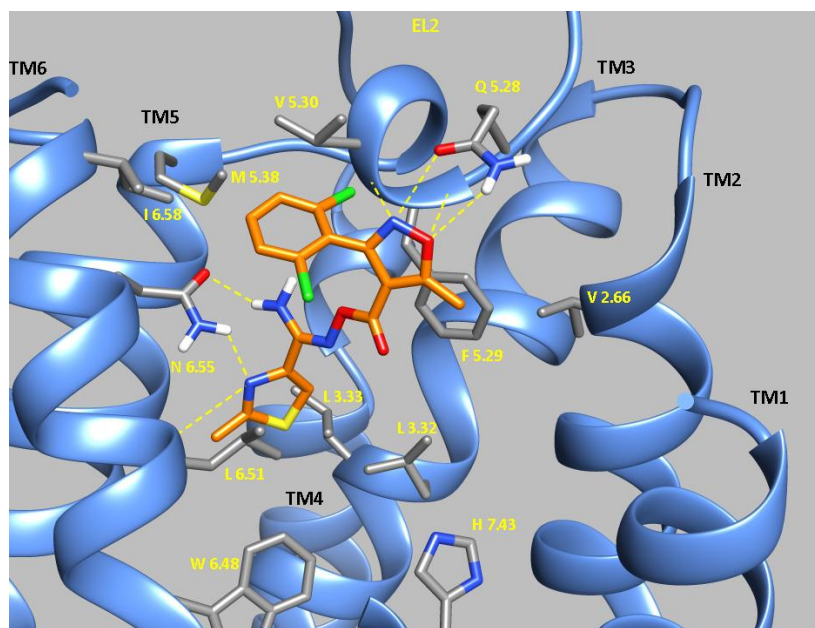
MD replica of a novel selective ligand inside the A_3AR orthosteric binding area